

Mixing in flows down gentle slopes into stratified environments

By PETER G. BAINES

CSIRO Atmospheric Research, PMB No. 1, Aspendale 3195, Australia

(Received 15 November 1999 and in revised form 13 February 2001)

Observations of the flow of dense fluid into uniformly density-stratified environments down plane slopes with small inclination to the horizontal ($\leq 20^\circ$) are described, and a quantitative model for such flows is presented. In these experiments the dense fluid is released at the top of the slope for a finite period of time. The resulting downslope gravity current, or downflow, has uniform thickness with a distinct upper boundary, until it approaches its level of neutral density where the fluid leaves the proximity of the slope. Turbulent transfers of mass and momentum occur across the upper boundary, causing a continuous loss of fluid from the downflow in most cases, and associated loss of momentum. The flow may be characterized by the local values of the Richardson number Ri , the Reynolds number Re (generally large), and of $M = QN^3/g'^2$, where Q is the (two-dimensional) volume flux, N the buoyancy frequency and g' the (negative) buoyancy of the dense fluid. The model for the downflow describes the turbulent transfers in terms of entrainment, detrainment and drag coefficients, E_e , E_d and k respectively, and the observations enable the determination of these coefficients in terms of the local values of M and Ri . The model may be regarded as an extension of that Ellison & Turner (1959) to stratified environments, describing the consequent substantial changes in mixing and distribution of the inflow. It permits the modelling of the bulk properties of these flows in geophysical situations, including shallow and deep flows in the ocean.

1. Introduction

Gravity currents are flows of dense fluid driven by the difference in buoyancy between this fluid and its environment, and they are quite common in nature (see for example Simpson 1997). Many of these natural phenomena occur over sloping terrain, which increases the driving force of buoyancy. Prominent examples include nocturnal flows down hillsides, powder snow avalanches, overflows in the ocean such as the Mediterranean and Bass Strait outflows, and the flow of cold river water into lakes. Such flows are generally at large Reynolds numbers, and are highly turbulent. Consequently, the most effective way to study them is often in the laboratory, where they may be generated fairly easily. This paper presents an experimental study of such flows for small slope angles (here defined to be less than about 20°), focusing on the mixing properties associated with them. Most bottom slopes in the ocean lie within this range of slope angles, so that the results are relevant to oceanic situations. In contrast to previous experiments of this type, the environmental fluid here is stratified, and this causes substantial changes to the turbulent eddies and mixing associated with the downflow.

A sudden onset of a steady source of dense fluid at the top of the slope produces a gravity current that is led by a relatively large 'head' of dense fluid, and this head is

associated with considerable mixing with the environmental fluid (Britter & Linden 1980). For a downslope gravity current caused by the sudden onset of a steady line source (density ρ_i) flowing into a homogeneous environment, this head is observed to move at a uniform speed U_f that is weakly dependent of the slope angle θ , and depends on the initial volume flux Q_0 (per unit slope width) and buoyancy g'_0 in the form

$$U_f \approx a(g'_0 Q_0)^{1/3}, \quad g'_0 = g \frac{\Delta\rho}{\bar{\rho}}, \quad (1.1)$$

where $1 < a < 1.8$ depending on slope angle, g is acceleration due to gravity, $\Delta\rho$ is the difference in density between the inflowing and environmental fluid, and $\bar{\rho}$ is the mean density of the two. The following downslope flow travels more rapidly by a factor of approximately 1.7 (Britter & Linden 1980), and the size of the head increases with time due to this supply of fluid from behind and to inherent mixing with the environment. This rate of increase of the size of the head increases approximately linearly with slope angle.

Observations of the flow following the head have been described by Ellison & Turner (1959), who derived a dynamical model for the bulk properties of the flow, based on measurements over a broad range of parameters. They showed that the mean fluid velocity is independent of downslope distance, and is dependent on slope angle, or more particularly, on the local bulk Richardson number, Ri , which is approximately uniform with downslope distance. Following the work of Morton, Taylor & Turner (1956) on vertical buoyant plumes, Ellison & Turner introduced the concept of *turbulent entrainment* for downslope flows. This involved the assumption that the turbulence and associated mixing in the downflowing current would cause a net motion of environmental fluid towards and into the current, at a local speed that was proportional to the local mean downslope velocity of the current. The constant of proportionality is known as the *entrainment constant*, E . This is essentially a dynamical similarity assumption, but it is plausible because environmental fluid that is mixed with the downflow becomes denser than the environment, and hence will also flow in the downslope direction. Ellison & Turner showed that E is dependent on the local Richardson number, and incorporated this into a mathematical model for the mean properties of the flow, as described in more detail in §3. This kind of model has been widely used to describe downslope flow in the atmosphere and ocean, with varying success (see for example Smith 1975; Manins & Sawford 1979; Price & Baringer 1994).

The experiments of Ellison & Turner were for a homogeneous environment, but the model equations derived from their experiments may be rescaled to include a stratified environment (Turner 1986) if one assumes that the same physical processes are operating, in the manner that was done for plumes by Morton *et al.* (1956). On this basis, this model has been used to describe flows into stratified environments, but the present experiments show that this is inappropriate.

The first experiments on downslope flows into continuously stratified environments were described by Mitsudera & Baines (1992). Here there is an additional parameter, N , the buoyancy frequency of the initial density stratification $\rho_0(z)$ which was uniform in these experiments, and in the work described in this paper. A related important parameter is D , the depth below the source where the initial density of the fluid in the tank equals the inflow density. They are related by

$$N^2 = -\frac{g}{\bar{\rho}_0} \frac{d\rho_0(z)}{dz} = \frac{g'_0}{D} = \frac{g\Delta\rho_0(0)}{D\bar{\rho}_0}, \quad (1.2)$$

where the vertical coordinate z is measured from the level of the source, at the top of the slope, and $\Delta\rho_0(0)$ denotes the difference in density between the inflowing and environmental fluid at this level. This system is governed by four main dimensionless parameters: the slope angle θ , and the Richardson number Ri_0 , the Reynolds number Re , and a parameter M_0 , defined by

$$M_0 \equiv \frac{Q_0}{(g'_0 D^3)^{1/2}} = \frac{Q_0 N^3}{g_0'^2}, \quad Ri_0 = \frac{g'_0 \bar{d}^3 \cos \theta}{Q_0^2}, \quad Re = \frac{Q_0}{\nu}, \quad (1.3)$$

where ν is kinematic viscosity and \bar{d} is the mean thickness (averaged over waves and eddies) of the downflowing current. \bar{d} is an observable property of the flow that is determined by the other parameters and is largely independent of downslope distance s in the region of interest, as shown in the following sections. M_0 and Ri_0 are determined by the initial conditions for the downflow, and these parameters may be generalized to characterize the current at any height z by defining

$$M = \frac{QN^3}{g'^2}, \quad Ri = \frac{g' \bar{d}^3 \cos \theta}{Q^2}, \quad (1.4)$$

using local values of Q , N and

$$g'(z, t) = \frac{g \Delta\rho(z, t)}{\bar{\rho}}, \quad (1.5)$$

where $\Delta\rho(z, t)$ is the difference between the mean density of the downflow at height z , and the environmental fluid at the same level. $M = 0$ corresponds to a homogeneous environment, and M increases with increasing stratification, although $M(0) \equiv M_0 < 1$ for realistic flows in these experiments.

Mitsudera & Baines (1992) carried out experiments with a slope angle of $\theta = 6^\circ$, and $Re > 300$, and described some properties of the turbulent downflow and the mixing process that occurred above it. Their observations showed that for 6° slopes the motion of the initial head was described well by (1.1), until the head approached its level of neutral buoyancy. The gravity current following this head had conspicuous small-scale mixing taking place at its upper boundary, but otherwise it had a well-defined mean velocity and thickness. Further, it was noted that, in addition to the main horizontal plume of fluid leaving the slope near the point where the dense fluid reached its ambient density, there was a second, broader, weaker plume higher up, fed by a complex three-dimensional circulation emanating from the mixing region above the downflow. The vertical distance over which these downslope flows were observed was relatively small (20 cm from shelf to bottom of tank), and this made some aspects of the interpretation uncertain. The experiments described in the present paper were carried out with a longer slope, and covered a range of slope angles from 3° to 12° , with some supplementary experiments on slopes of 20° . Flows down steeper slopes have different properties, and will be described elsewhere. Attention here is focused on the bulk properties of the main current, the effect of stratification on entrainment into the current and its converse, 'detrainment' of fluid from it into the environment. As shown below, the mean properties of the current including these features may be inferred from density soundings taken before and after the experiment. In this paper, I next describe the experiment and techniques involved, and then proceed to the development of the theoretical model for the downslope flow, and the analysis and interpretation of the results. An early version of some of these results, restricted to experiments at $\theta = 6^\circ$, was presented at the IMA Conference on Stratified Flows

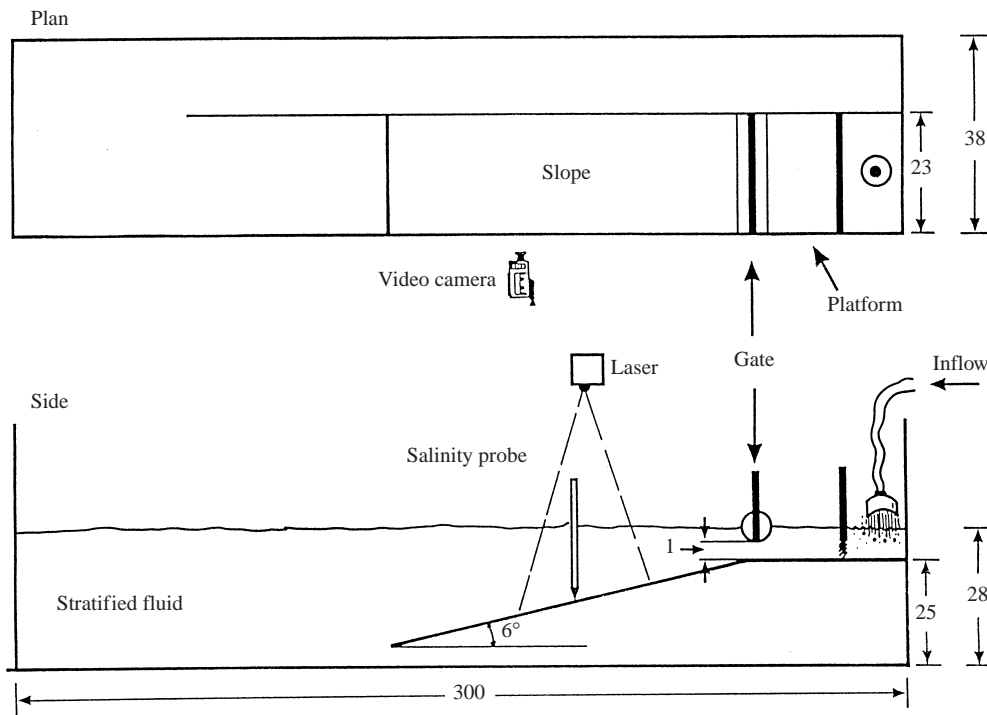


FIGURE 1. Plan and side views of the tank used in these experiments, showing the configuration for the 6° slope. A central vertical section of the flow on the slope was illuminated by a thin sheet of laser light from above, and video-recorded by viewing from the side. Only part of the total width of the tank was used, which enables the simulation of an effectively longer tank for these experiments. All measurements in cm.

in Dundee, September 1996, and published as Baines (1999). Experiments on flows descending through a density interface have recently been described by Monaghan *et al.* (1999), but the processes observed there differ substantially from those described here.

2. The experiment and qualitative observations

The experiments were carried out in a glass-sided tank as illustrated in figure 1. This tank was rectangular in cross-section, 80 cm high with internal dimensions of 299 cm in length and 38 cm in width, open at the top and with a solid horizontal bottom. The effective working length of the tank was extended by the device of inserting a thin vertical Perspex partition, extending from one end to a point 25 cm short of the other end, and with a uniform gap of 23 cm on one side and 15 cm on the other. The main working region of the tank was in the wider region of width 23 cm, and the experiment was made two-dimensional in this region as much as possible. For the low-frequency motions and changes produced in the ambient stratification, the fluid behind the partition could be regarded as a two-dimensional extension of the working region. A horizontal platform or shelf 40 cm long with a plane downward sloping extension 2 m in length was inserted at the closed end of this region. The height of the horizontal platform varied from 20 to 40 cm depending on the slope angle. A number of different slope angles were used, principally 3° , 4.5° , 6° and 12° , to the horizontal, with some additional runs at 20° . There was a fixed sluice-type gate

	M_0	Q_0 ($\text{cm}^2 \text{s}^{-1}$)	g'_0 (cm s^{-2})	N (s^{-1})	D (cm)	Re $= Q_0/\nu$	\bar{d} cm($\pm 15\%$)	Ri_0	$ Z_b $
(a)	0.0130	1.32	13.01	1.19	9.2	132	0.8	3.82	0.9
	0.0150	1.32	9.29	0.99	9.4	132	0.74	2.15	0.86
	0.0408	2.73	4.49	0.67	10.0	273	1.33	1.42	0.91
	0.0435	3.44	8.18	0.94	9.1	344	1.05	0.80	0.94
	0.0443	4.5	8.36	0.88	10.7	450	1.33	0.97	0.83
	0.0549	4.85	8.47	0.93	9.7	485	1.28	0.75	0.89
	0.1016	8.39	8.95	0.99	9.1	839	1.4	0.35	0.8
	0.1625	12.62	8.17	0.95	9.0	1262	1.61	0.21	0.8
	0.1858	12.62	7.38	0.929	8.55	1262	1.92	0.328	0.965
	0.1929	17.14	8.95	0.96	9.6	1714	2	0.24	0.83
	0.2215	15.45	6.41	0.84	9.1	1545	2.2	0.29	0.875
(b)	0.0089	1.32	9.04	0.819	13.46	132	0.36	0.241	0.93
	0.0291	4.15	8.84	0.818	13.21	415	0.88	0.349	0.898
	0.0423	6.97	9.32	0.808	14.28	697	0.99	0.186	0.874
	0.0697	10.5	9.53	0.844	13.36	1050	1.21	0.153	0.902
	0.0768	6.97	5.85	0.723	11.21	697	1.4	0.330	0.825
	0.0876	12.62	8.06	0.767	13.71	1262	1.47	0.16	0.896
	0.1485	9.79	3.51	0.572	10.74	979	1.75	0.196	0.856
(c)	0.0012	0.401	26.96	1.29	16.3	40	0.4	10.7	
	0.0025	1.11	27.65	1.20	19.2	111	0.5	2.81	0.93
	0.0036	1.82	30.04	1.21	20.4	182	0.5	1.13	0.954
	0.0062	2.67	29.61	1.27	18.5	267	0.5	0.52	0.971
	0.0068	3.44	31.61	1.26	20.0	344	0.5	0.33	0.911
	0.0110	5.56	31.63	1.26	20.1	556	0.7	0.35	0.945
	0.0184	8.39	23.88	1.08	20.59	839	0.9	0.25	0.913
	0.0362	6.26	9.43	0.80	14.7	626	0.9	0.17	0.901
	0.0445	8.39	18.22	1.21	12.5	839	0.8	0.13	0.889
	0.0614	8.39	6.81	0.70	14.0	839	0.9	0.070	0.773
	0.0655	11.21	8.85	0.77	14.9	1121	0.9	0.051	0.755
	0.0932	11.21	5.75	0.65	13.6	1121	1.08	0.057	0.748
	0.0936	8.39	7.58	0.86	10.2	839	0.83	0.061	0.879
(d)	0.0010	0.966	26.7	0.884	34.2	96.6	0.35	1.20	0.971
	0.0026	2.733	28.1	0.913	33.7	273	0.65	1.01	0.936
	0.005	5.56	31.9	0.971	33.8	556	0.75	0.43	0.918
	0.0063	4.15	15.4	0.711	30.5	415	0.6	0.19	0.903
	0.0103	8.38	17.6	0.724	33.6	838	0.9	0.18	0.871
	0.0306	5.56	5.66	0.561	18.0	556	0.75	0.075	0.764
	0.0612	11.21	7.89	0.698	16.2	1121	0.92	0.048	0.739
	0.0794	11.21	5.46	0.595	15.4	1121	1.0	0.042	0.734
	0.0808	11.21	4.97	0.563	15.7	1121	1.22	0.070	0.69

TABLE 1. Parameters for the experiments (see text for the definitions), including the observed values of \bar{d} , Ri_0 and $|Z_b|$. (a) 3° slope, (b) 4.5° slope, (c) 6° slope, (d) 12° slope

consisting of a vertical barrier terminated at its bottom by a horizontal cylinder of radius 2 cm, leaving a gap of (typically) 1 cm above the horizontal platform below. For the slope angles of 6° and 12°, this barrier was located 31 cm from the endwall, and for slope angles of 3°, 4.5° and 20°, it was at 39 cm from the endwall. Before each experiment the tank was filled with stratified fluid to a level above this gap.

During the experiment, dense fluid was supplied by a hose from an external reservoir to an area behind a region of wire mesh on the platform near the end of the tank,

behind the sluice gate. This wire mesh was inserted to make the supply approximately uniform across the width of the tank. An additional solid barrier was inserted between the wire mesh and the sluice gate prior to each run. The commencement procedure then consisted of the removal (by vacuum cleaner) of all ambient fluid behind this temporary barrier, and its subsequent replacement by dense fluid from the hose. When the surface of this dense fluid equalled that of the ambient fluid in the tank, the temporary barrier was removed, giving a sudden commencement at the removal time to the release of continuously supplied dense fluid. This fluid then flowed through the gap under the sluice barrier and down the slope as a gravity current. For runs with large flow rates at the smaller slope angles, where the observed value of \bar{d} is greater than 1 cm, the width of the gap was increased to 2 cm, in order to avoid hydraulic jumps occurring immediately downstream. Such jumps are undesirable because the mixing associated with them corrupts the experiment, and several runs had to be discarded for this reason.

At the start of an experiment, the tank was filled with density-stratified fluid that was produced by the familiar two-tank mixing procedure with salt water. This filled the whole of the tank including the region on the far side of the Perspex partition and the region underneath the slope and horizontal platform. The purpose of this was to have an approximately uniform stratification in the tank, by having a horizontal cross-sectional area that was uniform with height during filling. After filling, the gaps connecting the region beneath the slope and platform were closed and sealed, so that the fluid there was isolated and not involved in the subsequent experiment. After these gaps were closed and all motion due to filling had subsided, the vertical density profile was measured by a conductivity probe that was calibrated at the top and bottom by samples measured in an Anton Paar densitometer. This profile was designated $\rho_0(z)$, with z positive upwards and the origin taken at the level of the platform of the source.

The main experiment was performed by suddenly releasing dense fluid of density ρ_i at the top of the slope in the manner described above. This inflow was continued at a constant rate that was set and monitored by a flow meter in the inflow hose, and lasted for a fixed time that depended on the flow rate and ranged between 2 and 6 minutes. Various values of the inflow rate, inflow density and initial density gradient were used in a variety of experiments for each slope angle, and the details of these are given in table 1(a-d) which contain values of the controlling parameters and some key observations. The inflowing fluid was dyed with fluorescein, and illuminated in a thin central vertical section by a scanned beam from an argon ion laser, which gave a clear picture of a vertical cross-section of the motion. This cross-section was recorded on video tape for at least part of most runs. Overall observations of these flows showed that they had the general character of a gravity current flowing down the slope, with a broadly two-dimensional form and a distinct upper boundary where

FIGURE 2. A time sequence of the development of the flow for a typical experiment at $\theta = 6^\circ$, with the inflowing dense fluid dyed with fluorescein ($M_0 = 0.0058$, $Re = 273$). These pictures show instantaneous vertical sections near the centreline of the tank, illuminated by a thin vertical sheet of light from a scanned laser beam. Frames (a) and (b) show the initial gravity current head, and (d) is at a much later time than the first three. Frames (b-d) show the steady dense downflow with its main outflow at the bottom, and the growth of mixed, detrained fluid over the range of depths between the level of the source and this main outflow. The accumulation of detrained fluid is seen in the increasing intensity of the dye in the region above the main downflow, which slowly moves to the left.

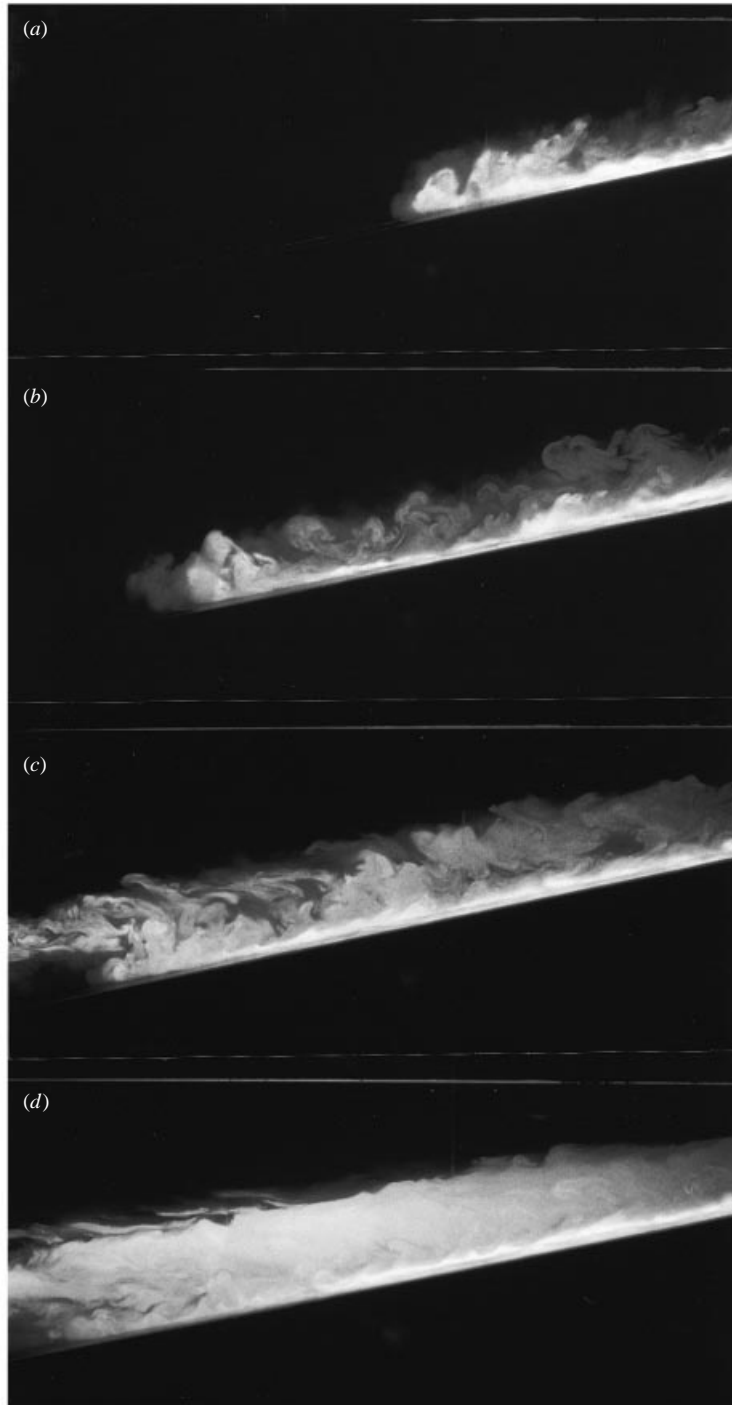


FIGURE 2. For caption see facing page.

turbulent mixing occurred. This flow had the initial familiar head structure (Britter & Linden 1980) with the approximately steady (in the mean) current following. Figure 2 shows a time sequence during the early stages of a typical run at $\theta = 6^\circ$, and the gravity current head is seen in the top frame. Compared with flows into homogeneous environments, these flows differ in that the fluid only penetrates to a level slightly above the level $z = -D$ where ρ_i equals $\rho_0(z)$, and this is denoted by the lowest levels reached by the dyed fluid in figure 2. During the downflow, dyed dense fluid mixed with some of the undyed environmental fluid, with the result that at the end of the run, all fluid that had come into contact with the inflowing fluid was 'tagged' and thereby identified as dyed fluid. In a typical run, when all motion had ceased, the dyed fluid was (often) concentrated at a level that was slightly above a vertical distance D below the level of the shelf, but it was also present throughout the depth range between the shelf and this level. This implied that some inflowing fluid had become mixed with its environment and found its own level somewhere above its initial density, and the process causing this was continuous in ρ and z . This process of fluid leaving the main current and entering the environment is termed *detrainment*, and its initial development can be clearly seen in figure 2.

Observations of the flow during the runs with $\theta \leq 20^\circ$ showed that three distinct regions of flow may be identified, as follows. In region I, occupying the first 3 cm or so in depth below the source, the flow emerges from the source region and adjusts to a mean state on the slope. For the runs where $Re < 700$ (approximately), the dense fluid emerges from under the sluice gate in an approximately laminar state. It then accelerates down the slope and two-dimensional Kelvin–Helmholtz billows form. This leads to irregular three-dimensional wave patterns on the interface and turbulence further down the slope. When $Re > 700$ (approximately), the flow is generally turbulent on exit, but in both cases the flow settles down to a mean state of uniform thickness of the downflowing layer. When this has become fully established the flow is identified as region II; here the mean layer thickness \bar{d} remains approximately constant with downslope distance, and this persists for most of the remainder of the downflow. This constancy of \bar{d} with s was tested by examining videotapes, and was found in all runs with the possible exception of some at 12° slope; in the latter, there was a suggestion of an overall decrease in \bar{d} of up to 20% over the length of region II. Figure 3 shows the form of the interface for three representative runs at slope angles of 3° , 6° and 12° . Several features can be seen in these instantaneous pictures. These include waves on the interface, wisps of fluid indicating fluid detrained from the dense layer, and evidence of this detrainment in the fluid above. The mean thickness \bar{d} of the downflowing current was measured from direct observations during the runs and also from videotape records. These mean values are given in table 1 (the runs at 6° are essentially the same as those described in Baines (1999), but some entries in table 1 of that paper differ slightly from table 1(c) here, because of minor corrections to the density and flow rate measurements). The flow at slope angle 3° is significantly less turbulent than that at the steeper angles, for the same values of M_0 .

Region II ends when the dense fluid approaches its neutral density level, and the layer thickens and spreads into the environment, forming region III; \bar{d} therefore reaches a potentially large value in this region. Below region III the fluid is undisturbed for $\theta \leq 20^\circ$, but for $\theta \geq 30^\circ$ there is a region IV in which the downflow overshoots its neutral level because of its inertia, and then returns. It should be reiterated that in each of these runs, there was an extensive central region between the initial adjustment region (region I) and region III below, in which no systematic trend in \bar{d} with downslope distance could be discerned. There was, however, general unsteadiness

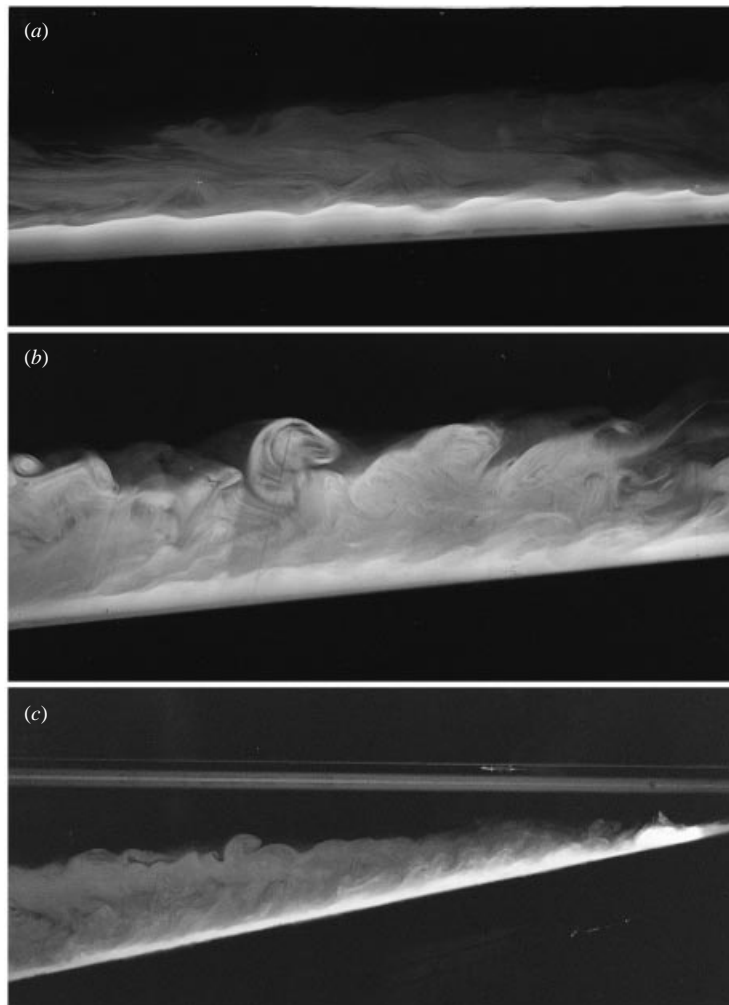


FIGURE 3. Photographs showing the central region (region II) of three typical downflows for different slope angles, each taken during the middle (approximately) of the run period. (a) 3° slope, $M_0 = 0.011$; (b) 6° slope, $M_0 = 0.083$; (c) 12° slope, $M_0 = 0.021$. As in figure 2 the inflowing fluid has been dyed with fluorescine, and the laser illumination shows a vertical section. Note the sharp upper boundary of the dense main current, as in figure 2, and the variation with slope angle. In (a) and (b) all the flow lies in region II, whereas in (c) region I is visible at the top of the slope.

in these downflows, with continual wave motion and turbulence on short length and time scales, and consequent uncertainties in the observations of \bar{d} .

Figure 4 presents quantitative examples of flow at 6° slope, showing velocity profiles (measured by bead tracking) and a density profile (measured by conductivity probe) at various positions on the slope. These are effectively instantaneous sample observations (particularly for velocity), and are only indicative of the mean profiles. However, they illustrate the sharpness of the interface, and the contrast between the dense flowing layer and the relatively stationary fluid above it.

In summary, region I denotes the region of adjustment from the sluice gate to the 'steady state' of region II, which is the main region of the downflow. Region III denotes the termination of this region, where the remaining fluid (if any) in the

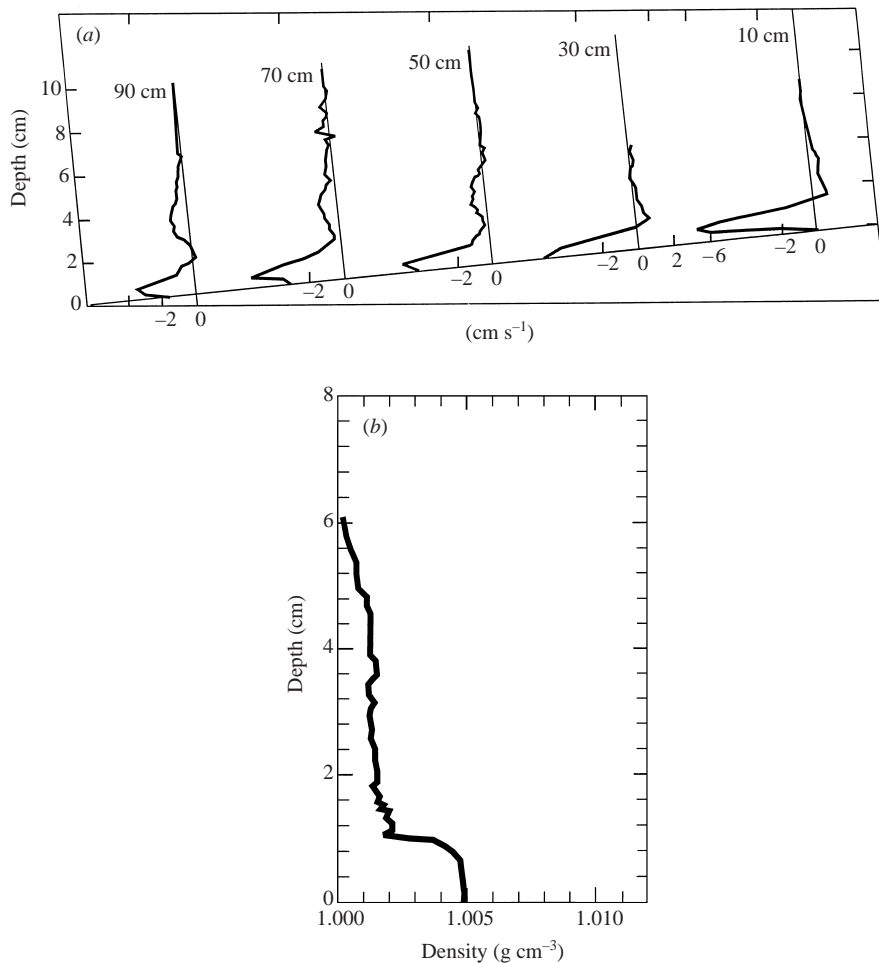


FIGURE 4. (a) Nearly steady velocity profiles measured by particle tracking of tracers illuminated by a thin laser sheet. The slope is 6° , with $M_0 = 0.02$, $Re = 290$. The main downflow is clearly seen, although the shape of the profile is variable because of the limited resolution of the technique. An upper level outflow of detrained fluid is also evident. Distances marked denote downslope distance of the measured profiles from the top of the slope. (b) A typical density profile taken by a traversing conductivity probe during a run, showing the sharpness of the interface and the perturbed stratified region above. $M_0 = 0.05$, $Re = 273$.

downflow leaves the vicinity of the slope to find its ambient, neutral level. In region II there are three identifiable regions of fluid motion as one moves outward in a direction normal to the slope. First, there is the downslope-flowing region on the surface of the slope, with mean thickness \bar{d} , bounded above by a turbulent interface. Secondly, immediately above this current the flow is in a weakly turbulent state with relatively small velocities, but with a discernible three-dimensional mean flow structure (Mitsudera & Baines 1992). Here the mean density surfaces are observed to have a small upward inclination toward the current on the slope (see §4). Further away from the slope, the flow is laminar and the motion is nearly horizontal. The motion in these regions outside the main downflow is due to mass and buoyancy fluxes at the interface, which cause the fluid to move under gravity to its equilibrium density level in the environment.

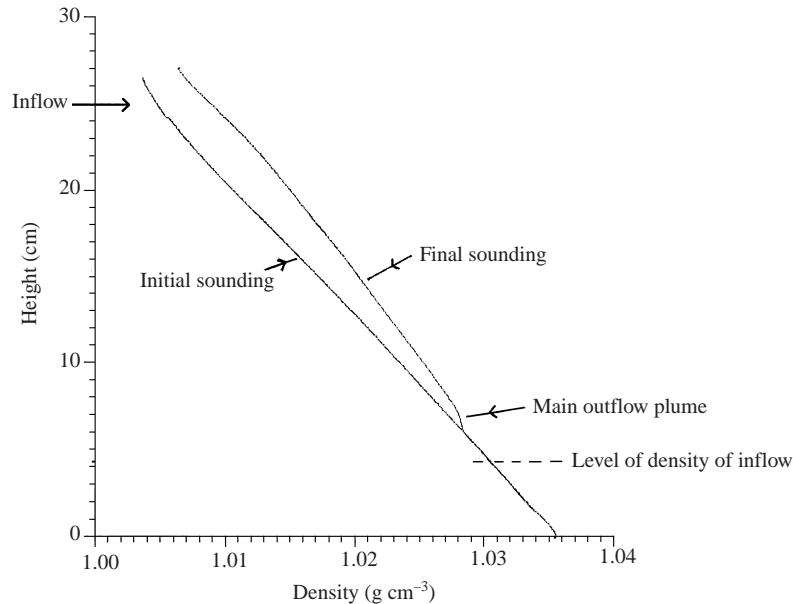


FIGURE 5. Initial and final density soundings for the run with $\theta = 6^\circ$, $M_0 = 0.0184$. These profiles were taken when the fluid in the tank was effectively at rest, and this figure shows the nature of the differences between the profiles for all runs. Here the height coordinate denotes height above the floor of the tank.

After the inflow ceased, some motion persisted in the form of low-frequency internal waves in the tank, which took up to 30 minutes to decay through viscous dissipation. When all this motion had died away after a downflow event, the density profile was again measured (several times) by the same techniques and with the same accuracy as the initial density profile, and the comparisons between these two profiles constitute the main quantitative data from the experiment. An example of initial and final density profiles is shown in figure 5. The conductivity probe was re-calibrated at the end of the experiment. Generally this showed slight differences from the calibration at the beginning of the experiment, so that the mean of the two could be used for all initial and final profiles, except for a small constant offset that implied a uniform drift in the probe apparatus. This was removed by equating the signal in the 'before' and 'after' profiles in the fluid near the bottom of the tank, well below the active levels of the experiment, where the density was not affected by the downflow. The length of time for each run was determined by three factors. First, it needed to be long enough to give measurable differences between the two profiles. Secondly, it is necessary to minimize the effect of the head relative to that of the following current, whose effect increases with time. Thirdly, it should be short enough that the net inflow was not so large as to displace the mean isopycnals too far from their initial positions relative to the topography, to invalidate the differencing process. It was for this reason that the volume of the host fluid in the tank was made as large as possible, to increase the running time, by including the region of the tank behind the partition, as described above. Only one run could be carried out with each stratified fill, implying at most one run each day, so that a considerable amount of time and effort was required to accumulate data from a sufficiently large range of parameter values.

The observed values of \bar{d} shown in table 1 enable the calculation of the local bulk Richardson number based on the local volume flux Q and the local density difference

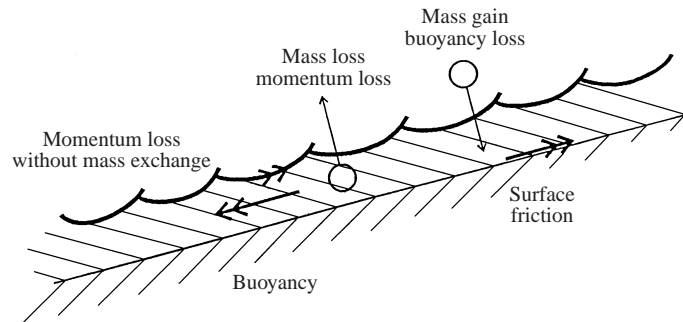


FIGURE 6. Physical processes associated with the derivation of equations (3.24)–(3.26).

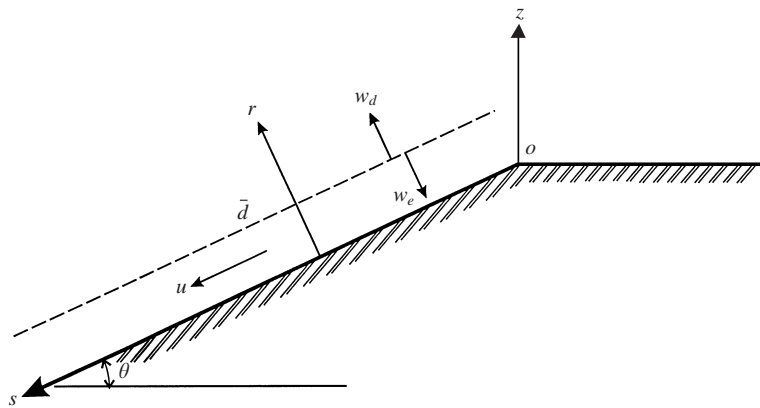


FIGURE 7. Coordinates and notation for the downslope flow model of § 3.

$\Delta\rho$, defined by (1.4). Values of Ri at the top of the slope, using Q_0 and $\Delta\rho_0$, are denoted Ri_0 as defined by (1.3), and are also given in the table.

3. Theoretical analysis—models for downslope flow

We first describe the conceptual model and equations that are used to interpret the observations. This model describes the bulk characteristics of a downslope flow, as do most previous models, but here we allow for two-way exchange between the current and its environment, as the observations described in § 2 imply. This requires careful definition and analysis of the quantities involved. A schematic diagram illustrating the physical processes affecting the downflow, and incorporated in this model, is shown in figure 6. We take a plane slope at angle θ to the horizontal with axes as shown in figure 7, with s directed downslope and r normal to it, and with a current of dense fluid of thickness $d(s, t)$ and velocity $u(r, s, t)$ in the s -direction and $w(r, s, t)$ in the r -direction. These flows are generally turbulent, with waves and eddies on the interface, but for present purposes we are interested in the mean values on longer time scales than those of these eddies. Hence we define

$$d = \bar{d} + d', \quad u = \bar{u} + u', \quad w = \bar{w} + w', \quad (3.1)$$

where the overbar denotes averages over time scales much longer than that of the eddies, and the averages of u' and w' are zero; \bar{d} denotes the observed mean position of the interface, but the mean value of d' is in general non-zero, as described below.

The surface $r = d(s, t)$ is a material surface at any given instant, but as observed in the experiments it does not remain continuous. Folds and extensions appear in it, and small loops and wisps break off carrying fluid in both directions. Hence fluid moves across the interface, detrained fluid leaving the dense layer with a net velocity represented by w_d , and entrained fluid entering it with a velocity represented by w_e , where w_d is positive upwards and w_e positive downwards (in the direction of r decreasing). \bar{d} defines the mean position of this surface, which is identified with the mean position of the observed surface in the experiments. If $r = d$ is assumed to be a continuous material surface, we have

$$w(d, s, t) = \frac{\partial d}{\partial t} + u(d, s, t) \frac{\partial d}{\partial s} = - \int_0^d \frac{\partial u}{\partial s} dr, \quad (3.2)$$

so that

$$\frac{\partial d}{\partial t} + \frac{\partial}{\partial s} \int_0^d u dr = 0. \quad (3.3)$$

However, if $r = \bar{d}$ is the mean position of the interface, the observation that there is net transfer of fluid across this level implies that \bar{d}' is in general not constant, and that (3.3) should be replaced by

$$\frac{\partial \bar{d}}{\partial t} + \frac{\partial Q}{\partial s} = - \frac{\partial \bar{d}'}{\partial t} = -\bar{w} = -(\bar{w}_d - \bar{w}_e), \quad (3.4)$$

where Q is the total downslope flow, given by

$$Q(s, t) = \int_0^d u dr. \quad (3.5)$$

From dimensional analysis, following Ellison & Turner (1959) and List & Imberger (1973) we expect the turbulent transfer term $\partial \bar{d}' / \partial t$ to scale with the mean velocity Q / \bar{d} , with a factor that depends on dimensionless quantities. Hence we write

$$\frac{\partial \bar{d}}{\partial t} + \frac{\partial Q}{\partial s} = (E_e - E_d) \frac{Q}{\bar{d}}, \quad (3.6)$$

where

$$\bar{w}_e = E_e Q / \bar{d}, \quad \bar{w}_d = E_d Q / \bar{d}, \quad (3.7)$$

and E_e and E_d are positive entrainment and detrainment coefficients, with forms yet to be determined. Note that if the two processes of entrainment and detrainment exactly cancel, there is no net flux across the interface but there is still a loss of dense fluid from the current, and a flux of environmental fluid into it.

The density field may be written in the form

$$\rho(r, s, t) = \bar{\rho}_0 + \frac{d\rho_0}{dz} (r \cos \theta - s \sin \theta) + \Delta\rho(r, s, t), \quad (3.8)$$

where $\rho_0(z)$ is the ambient stratification in the tank, $\bar{\rho}_0$ is a mean density and $\Delta\rho(r, s, t)$ is the increment in density of the dense fluid in the downflow. Writing (as in (1.5))

$$g'(r, s, t) = \frac{g\Delta\rho}{\bar{\rho}_0}, \quad (3.9)$$

conservation of mass ($D\rho/Dt = 0$) for an incompressible fluid then gives

$$\frac{\partial g'}{\partial t} + \frac{\partial}{\partial s} (ug') + \frac{\partial}{\partial r} (wg') = N^2 (w \cos \theta - u \sin \theta), \quad (3.10)$$

where N is the buoyancy frequency, given by $N^2 = -(g/\bar{\rho}_0)(d\rho_0/dz)$. Integrating over the depth of the dense layer then gives

$$\begin{aligned} \frac{\partial}{\partial t} \int_0^d g' dr + \frac{\partial}{\partial s} \int_0^d u g' dr + g'(d) \left(w(d) - u(d) \frac{\partial d}{\partial s} - \frac{\partial d}{\partial t} \right) \\ = N^2 \left(\cos \theta \int_0^d w dr - \sin \theta \int_0^d u dr \right). \end{aligned} \quad (3.11)$$

From (3.2), the third term (with $g'(d)$ as a factor) vanishes for a continuous material surface but, as discussed above, this surface is in general not continuous and there is a two-way flux across it. Fluid leaving the current has the momentum and buoyancy of the downflow, whereas fluid entering it is assumed to have zero momentum and the density of the environment, implying zero buoyancy. Hence, with these entrainment and detrainment processes present, taking the mean of the third term in (3.11) gives $\overline{g'(d)w_d}$, where $g'(d)$ denotes the density at the upper boundary, inside the current. The mean of the whole of (3.11), averaging over the eddies, then gives

$$\frac{\partial}{\partial t} G\bar{d} + \frac{\partial B}{\partial s} + \overline{g'(d)w_d} = -N^2 \left(\sin \theta \overline{\int_0^d u dr} - \cos \theta \overline{\int_0^d w dr} \right), \quad (3.12)$$

where G is the buoyancy and B is the buoyancy flux, given respectively by

$$G = \frac{1}{\bar{d}} \overline{\int_0^d g' dr}, \quad B = \overline{\int_0^d u g' dr}. \quad (3.13)$$

In particular, $G_0 = G(s=0) = g'_0$. We also have

$$\left| \overline{\int_0^d w dr} \right| \sim 0.5\bar{d}|\bar{w} + w_d - w_e| \ll Q \tan \theta, \quad (3.14)$$

given the smallness of the slope of the mean interface, and the entrainment and detrainment velocities (see below), and

$$\overline{g'(d)w_d} = E_d g'(\bar{d}) Q / \bar{d} = E_d G Q / \bar{d}, \quad (3.15)$$

since the entrained environmental fluid has zero buoyancy. Hence (3.12) may be written

$$\frac{\partial}{\partial t} G\bar{d} + \frac{\partial B}{\partial s} = -N^2 Q \sin \theta - E_d G Q / \bar{d}. \quad (3.16)$$

The equation of motion for flow in the dense layer, assuming hydrostatic pressure, is

$$\frac{\partial u}{\partial t} + \frac{\partial}{\partial s} u^2 + \frac{\partial}{\partial r} u w = -\cos \theta \frac{\partial}{\partial s} \int_r^d g' dr + g' \sin \theta + \nu \nabla^2 u. \quad (3.17)$$

Integrating across the thickness of the layer gives

$$\begin{aligned} \frac{\partial}{\partial t} \int_0^d u dr + \frac{\partial}{\partial s} \int_0^d u^2 dr = \sin \theta \int_0^d g' dr - \cos \theta \frac{\partial}{\partial s} \int_0^d r g' dr - u(d) \\ \times \left(w(d) - u \frac{\partial d}{\partial s} - \frac{\partial d}{\partial t} \right) - \tau(d) - \tau(0), \end{aligned} \quad (3.18)$$

where $\tau(d)$ and $\tau(0)$ denote frictional stresses on the layer at its upper and lower

boundaries respectively. The pressure gradient term is

$$\cos \theta \frac{\partial}{\partial s} \int_0^d r g' dr \approx \frac{1}{2} \cos \theta \frac{\partial}{\partial s} (\bar{d}^2 G) = O \left(\frac{1}{2} \cos \theta G_0 \bar{d} \sin \theta \frac{\bar{d}}{D} \right) \\ \ll G_0 \bar{d} \sin \theta \quad \text{if } \bar{d}/D \ll 1. \quad (3.19)$$

Hence this pressure gradient term is generally small compared with the buoyancy term $G\bar{d} \sin \theta$, but is included below for completeness. If we take the mean value of (3.18), averaging over the eddies as in (3.11), (3.15), we have

$$\overline{u(d) \left(w(d) - u \frac{\partial d}{\partial s} - \frac{\partial d}{\partial t} \right)} = \overline{u(d) w_d} = E_d Q^2 / \bar{d}^2. \quad (3.20)$$

Here, as for the buoyancy (in (3.11), (3.12)), the entrained fluid from outside the current is assumed to have zero (or at least negligibly small) downslope momentum, and hence the w_e term makes no contribution. Hence (3.18) becomes

$$\frac{\partial Q}{\partial t} + \frac{\partial S}{\partial s} = G\bar{d} \sin \theta - (k + C_{DL}) Q^2 / \bar{d}^2 - \frac{\cos \theta}{2} \frac{\partial}{\partial s} (\bar{d}^2 G), \quad (3.21)$$

where C_{DL} is the drag coefficient of the solid sloping bottom (and sidewalls), k is a drag coefficient for the overlying layer (with $\tau(0) = C_{DL} Q^2 / \bar{d}^2$, $\tau(d) = C_{DU} Q^2 / \bar{d}^2$), and

$$S = \overline{\int_0^d u^2 dr}. \quad (3.22)$$

If we assume that the downslope transport (of mass, momentum and buoyancy) by eddies within the current is small compared with that carried by the mean motion, we may write

$$S = Q^2 / \bar{d}, \quad B = QG. \quad (3.23)$$

If one also assumes that the mean state of the flow is steady with time, the bulk equations (3.6), (3.16) and (3.21) for the downflow may be written

$$\frac{\partial Q}{\partial s} = (E_e - E_d) Q / \bar{d}, \quad (3.24)$$

$$\frac{\partial}{\partial s} \frac{Q^2}{\bar{d}} = G\bar{d} \sin \theta - (k + C_{DL}) Q^2 / \bar{d}^2 - \frac{\cos \theta}{2} \frac{\partial}{\partial s} (\bar{d}^2 G), \quad (3.25)$$

$$\frac{\partial G}{\partial s} = -N^2 \sin \theta - E_e G / \bar{d}. \quad (3.26)$$

The equations (3.24)–(3.26) have been derived by using the qualitative features of the observations, and they will be used as a basis for quantitative interpretation of the experimental results. We note that these equations involve Q , G , \bar{d} , N and θ . From these we may construct the two dimensionless parameters M and Ri , as defined by (1.4). We do not expect E_e , E_d and k to be constant in general, but rather that they will be functions of the dimensionless parameters M , Ri , θ and Re . For the most part, we assume that Re is large enough for the flow to be sufficiently turbulent that the dependence on its value is minimal. Reynolds number effects are apparent in some runs with $Re < 200$, and these have been excluded from the analysis or treated with circumspection.

We may contrast the above model with the equations and model of Ellison & Turner (1959). In their model of dense downslope flows into a homogeneous environment,

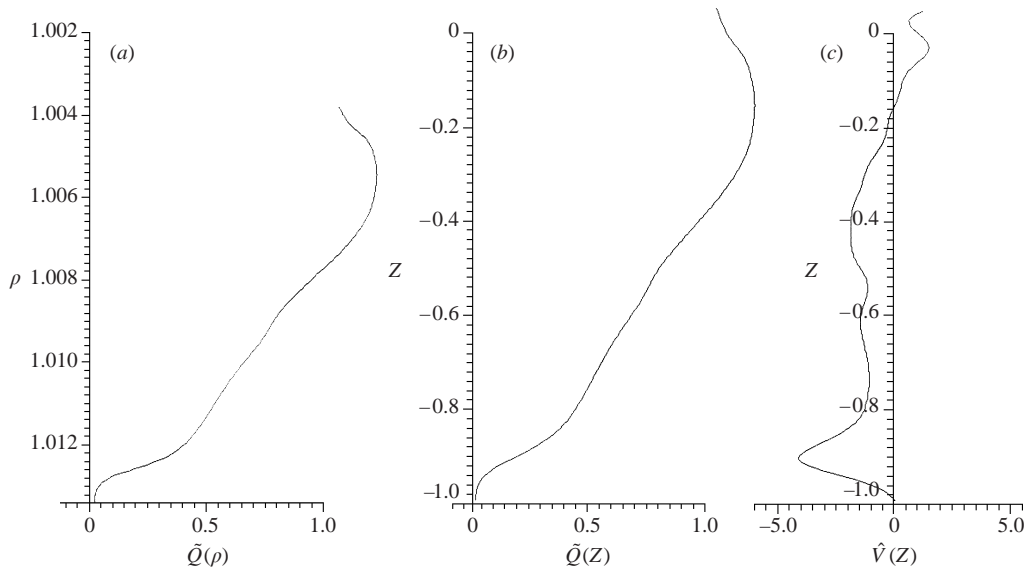


FIGURE 8. Representative example of the functions (a) $\bar{Q}(\rho)$, (b) $\bar{Q}(Z)$ and (c) $\hat{V}(Z)$, for the run with $\theta = 6^\circ$, $M_0 = 0.0362$. (a) The downslope volume flux is shown as a function of density, averaged over the whole downflow, and (b) and (c) show the corresponding mean downslope volume flux in the current and outflow velocity respectively, as functions of scaled depth $Z = z/D$. Positive values of $\hat{V}(Z)$ denote flow toward the slope.

there was no well-defined interface between the environment and the downflow. Instead, in a steady-state flow, the profiles of velocity and density perturbation extended further and further in the direction normal to the slope as one moved further downslope (see their figure 6, reproduced as figure 6.12 in Turner 1973). The variables corresponding to Q , B and S were defined as integrals in the r -direction from the slope to infinity. Growth in Q with distance downslope was interpreted as entrainment of the environment into this total flow, and the concept of detrainment did not enter the picture. The equations obtained comprised (3.24) above, with E_h (for homogeneous fluids) replacing $(E_e - E_d)$, (3.25) with the last two terms omitted, and $dB/ds = 0$. The entrainment coefficient E_h inferred from their experiments is larger than the values of E_e obtained here, because all environmental fluid that makes contact with the dense inflow is effectively entrained, by this definition. Nonetheless, as figure 4 of Ellison & Turner also shows, the dense, rapidly moving bottom current is still present in their experiments, and could in principle still be treated as a separate entity from the fluid above it.

4. Analysis of observations

The observations described in §2 yield the initial and final states of the stratification, before and after the downflow event. In these steady states the fluid properties are horizontally homogeneous. They would be the same if the tank geometry were altered to be two-dimensional, with the same area at each depth and a uniform width of 23 cm, and we assume this shape for the present analysis. At the depths occupied by the slope, the length of this hypothetical two-dimensional tank is

$$l(z) = 454.0 + z / \tan \theta \text{ cm}, \quad (4.1)$$

where z is the vertical coordinate measured from the level of the shelf as before, and has negative values in the region of interest. From the initial and final density profiles, such as those shown in figure 5, the increase in height of each density surface as a result of the downflow may be measured. The raw data of these profiles contain some small-scale noise, due to the slightly irregular motion of the probe during descent (scarcely visible in the unsmoothed profiles of figure 5). This noise can have an undesirable prominence when differences are taken, and hence it is removed by smoothing the profiles by using the Fourier transform based smoothing routine SMOOFT from Press *et al.* (1986). From the resulting initial and final heights for a given density value, a mean value of $l(z)$ is obtained from (4.1), and hence the increased volume of fluid below this density surface can be calculated. Dividing this by the effective running time of the inflow and the effective tank width then gives the mean downward flux across this density surface during the experiment, per unit width of the tank. Scaling this with Q_0 gives the function $\tilde{Q}(\rho)$, and an example is shown in figure 8(a).

From $\tilde{Q}(\rho)$ we may calculate the net downward flow at a fixed height z from

$$Q(z) = Q_0 \int_{\rho_i(z)}^{\rho_f(z)} \tilde{Q}(\rho) d\rho / (\rho_f(z) - \rho_i(z)), \tag{4.2}$$

$$\approx Q_0(\tilde{Q}(\rho_i(z)) + \tilde{Q}(\rho_f(z)))/2, \tag{4.3}$$

where $\rho_i(z)$ and $\rho_f(z)$ denote the initial and final density values at height z respectively. Expressing this in terms of $Z = z/D$, we have

$$\hat{Q}(Z) = Q(z)/Q_0, \tag{4.4}$$

where $\hat{Q}(Z)$ is therefore an appropriately stretched version of $\tilde{Q}(\rho)$. The mean outflow velocity $v(z)$ from the downflow (with the sign convention that v is negative for outflow) is then given by

$$v(z) = -\frac{dQ(z)}{dz}, \tag{4.5}$$

and in dimensionless form by

$$\hat{V}(Z) = v(z)D/Q_0 = -\frac{d\hat{Q}(Z)}{dZ}. \tag{4.6}$$

Examples of $\hat{Q}(Z)$ and $\hat{V}(Z)$ are shown in figure 8(b, c).

The initial and final density profiles thus give us the observed dependence of the downslope flux of fluid, and the net outflow from the current, with depth. There are two complicating factors that should be borne in mind when interpreting \hat{Q} and \hat{V} . First, as the dense fluid flows into the tank, the mean isopycnals rise according to the quantity of fluid that has penetrated below their level. The net rise is zero at the lowest level of penetration, and increases to a typical value of about 2–3 cm near the top of the slope at the end of a run. This changes the environmental stratification, but the effect is small, and has been neglected in the derivation of (3.24)–(3.26) where a stationary environment has been assumed. Secondly, visual observations during a run indicate that the mean position of the isopycnals near region II of the downflow are not exactly horizontal, but slope upward as they approach it. Hence the mean environmental density seen by the main downflow is slightly greater than that given by assuming a stationary environment. The reason for this is clear. In region II there is net detrainment (see below) of dense fluid, which leaves the current in the form

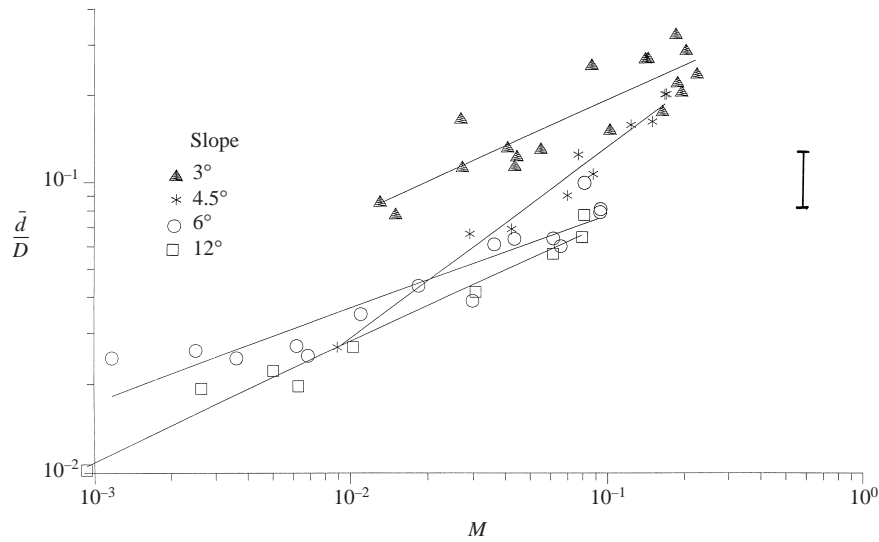


FIGURE 9. Dependence of the observed layer depth on M_0 for each slope angle. For constant, D , note the systematic decrease in \bar{d} with θ and increase with M_0 .

of thin wisps that mix with the environmental fluid, causing a slight increase in the local mean density of the latter. Hence the mean density surfaces slope upward close to the current. This effect appears to be small, and it has also been neglected in the derivation of equations (3.24)–(3.26).

There are, therefore, three main features of the observations that can be used to estimate the unknown quantities E_e , E_d and $k + C_{DL}$ in (3.24)–(3.26). These are: the constancy and value of \bar{d} , the level Z_b of the outflow of the remaining fluid at the bottom of the downflow, and the form of the profiles $\hat{Q}(Z)$ and $\hat{V}(Z)$. The observed values of \bar{d} are given in table 1, and are plotted in figure 9 as functions of M_0 and scaled with D . This shows that power law relationships of the form

$$\bar{d}/D = AM_0^\mu, \quad (4.7)$$

where A and μ are constants, exist for each slope angle. For any given value of M_0 , \bar{d}/D decreases with increasing slope angle from $\theta = 3^\circ$ to 12° , and this trend seems quite robust. The exponent μ varies from 0.35 (for $\theta = 6^\circ$) to 0.67 (for $\theta = 4.5^\circ$). Given the uncertainties in measurement ($\pm 15\%$) these differences may not be significant, as changing the value of an outlying point by this magnitude can significantly alter the value of the mean exponent. A mean value for μ over the four slope angles is 0.49.

Profiles of the net downslope flux $\hat{Q}(Z)$ as a function of depth (or downslope distance) for a representative selection of different M_0 values at slope angles of 3° , 6° and 12° are shown in figure 10, and (nearly) complete sets of the corresponding derivative functions $\hat{V}(Z)$ are shown in figure 11. These \hat{V} profiles denote the net outflow of fluid into the environment, as a function of depth. If there were no entrainment or detrainment in these downflows, the $\hat{Q}(Z)$ curves would be equal to unity for $-1 < Z < 0$, and zero for $Z < -1$. The $\hat{V}(Z)$ curves would then be zero for $Z < 0$, except for a negative delta-function 'spike' at $Z = -1$, so that the departure from these 'ideal' shapes gives a measure of the transfer properties between the dense downflow and its original environment. At the top of the slope we may expect that $Q(0) = Q_0$, and for $\theta = 3^\circ$ this is generally the case, except that $Q(0)$ is slightly larger

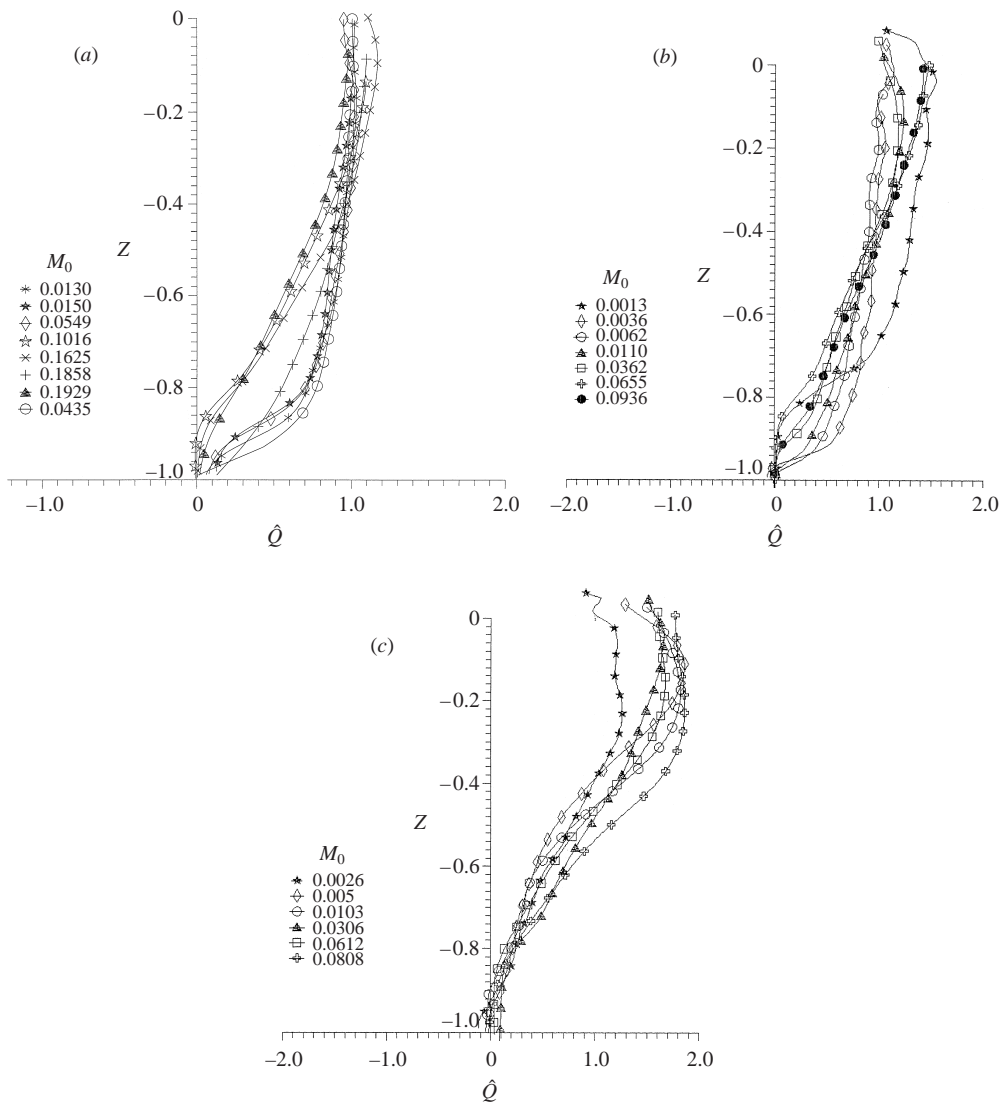


FIGURE 10. The downslope volume flux \hat{Q} as a function of depth Z for the slopes (a) 3° , (b) 6° and (c) 12° . Only a representative selection of runs are shown in each case, for clarity, and the symbols denote every tenth datum point.

than this for the larger Q_0 values. This is attributed to a small amount of entrainment in region I, near the gate. At greater depths in figure 10(a), a gradual decrease in $\hat{Q}(Z)$ is evident, and then a more rapid decrease to zero near the effective level of neutral buoyancy, Z_b . For small M_0 , the curves do tend to approximate the ‘ideal’ (no-mixing) shape, but as M_0 increases the decrease in net downflow occurs over a broader range of depths. The $\hat{V}(Z)$ curves for 3° slope (figure 11a) show a corresponding spike above $Z = -1$ for small M_0 , but the outflow becomes more extensive with increasing M_0 . A small amount of inflow due to initial entrainment near $Z = 0$ is also evident in some of these curves.

For the 6° slope, the $\hat{Q}(Z)$ curves for small M_0 are similar to those for the 3° case, and as M_0 increases, they evolve in a similar manner (the curve for $M_0 = 0.0013$ has

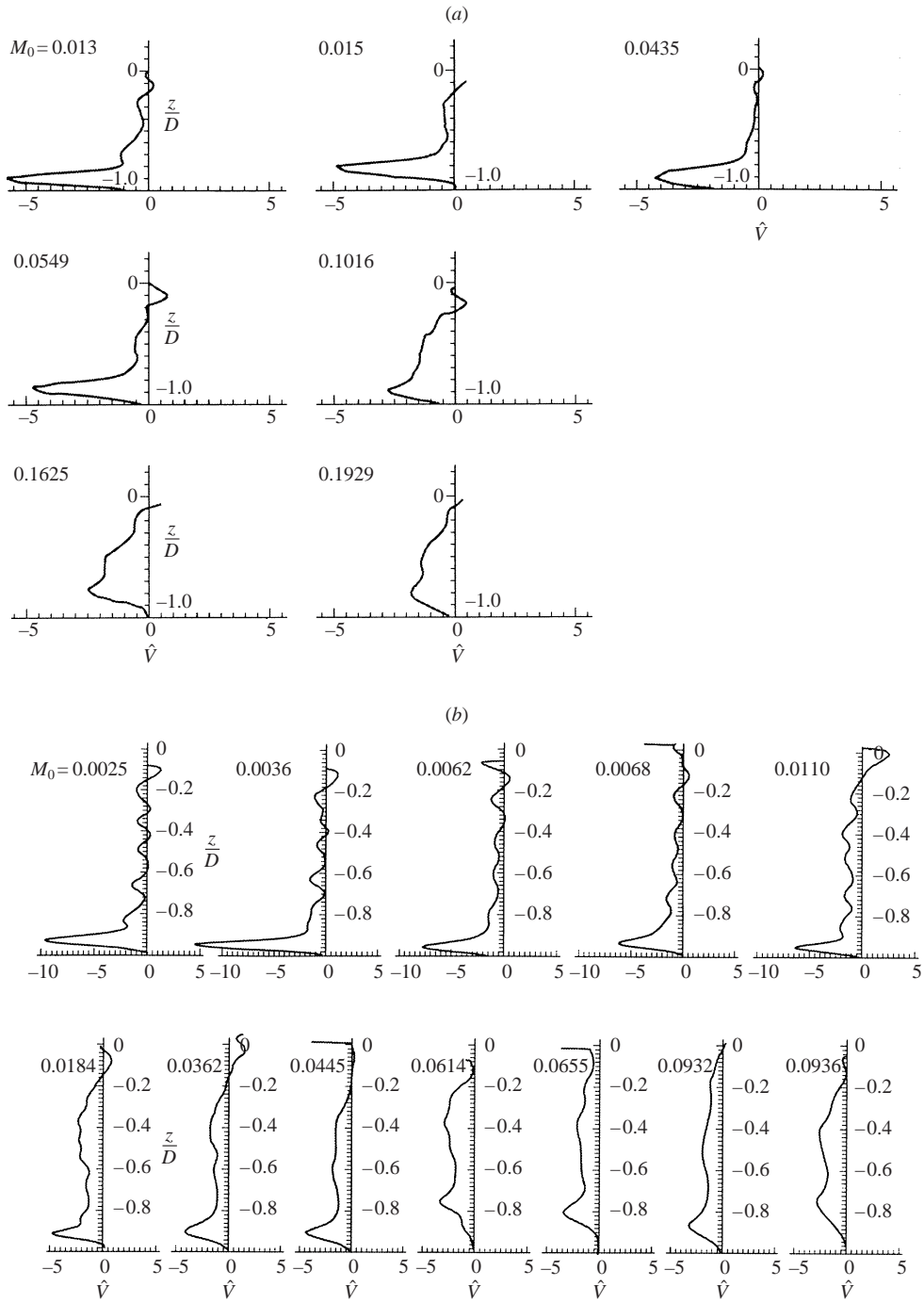


FIGURE 11 (a, b). For caption see facing page.

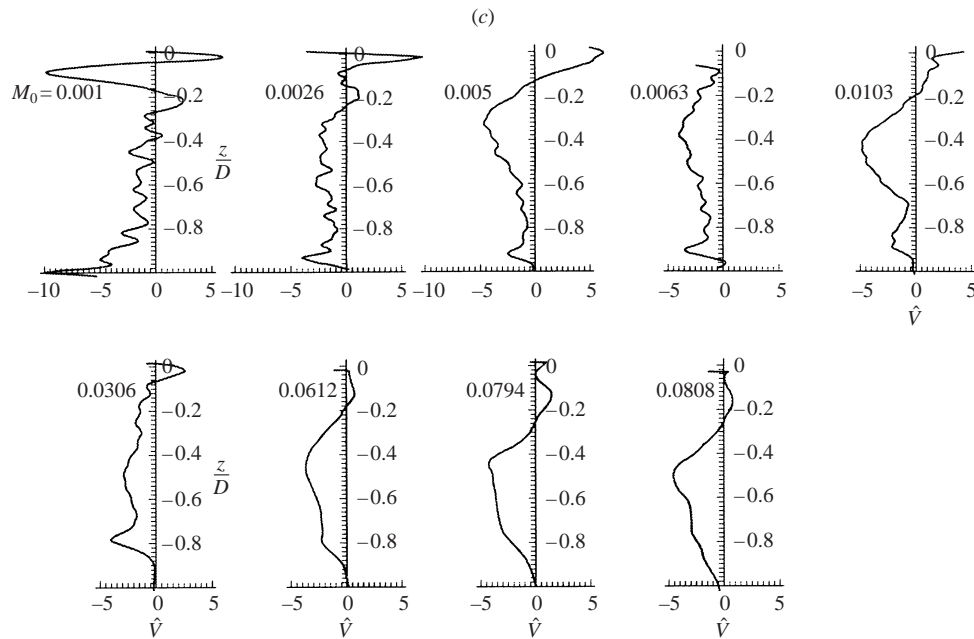


FIGURE 11. Profiles of the outflow function $\hat{V}(Z)$, obtained as the derivative of the curves in figure 8, for (a) 3° , (b) 6° and (c) 12° . Negative values imply flow away from the downflow. The curves are characterized by their M_0 values given in table 1.

an anomalously low Reynolds number ($Re = 40$), and is excluded from subsequent analysis). The $\hat{V}(Z)$ curves for the 6° slope (in figure 11b) for small M_0 show the expected shape except that there are small oscillations present over most of the length. These oscillations may also be seen in the $\hat{Q}(Z)$ curves, though they are less apparent, and after careful analysis they have been accepted as real. They progressively decrease in amplitude as M_0 increases, and are not evident for M_0 greater than 0.03. They are attributed to the effects of columnar disturbance modes in the stratification, which are forced by the large concentrated outflow near $Z = -1$; they are less conspicuous for the 3° experiments, apparently because the main outflow (scaled with D) is broader there. This concentrated outflow may be regarded as an intrusion layer into the stratified environment, and such intrusions are known to excite columnar disturbance modes, where the mode with largest amplitude has the vertical scale of the intrusion itself (Imberger, Thompson & Fandry 1976; Wong 1998). Such modes cause nearly steady motions in the stratified fluid above the downflow, and this pattern of motion apparently causes the variations in the detrainment shown by these curves. Like the 3° slope, the $\hat{V}(Z)$ curves for 6° also show the main peak in outflow becoming less pronounced and generally occurring at higher locations as M_0 increases.

The 6° runs have \hat{Q} values larger than unity near the top of the slope for larger M_0 values (figure 10b). In some cases $\hat{Q}(0)$ reaches magnitudes of 1.5, implying that the net downflow at the top of the slope has increased by up to 50%. This is due to increased initial mixing in region I, and is reflected in the inflow at upper levels seen in the \hat{V} curves. These curves also show an upper level peak in the outflow (near $Z \approx -0.4$), that is interpreted as this fluid mixed in region I finding its neutral level. For the purposes of estimating the entrainment and detrainment coefficients, this initial mixing is an undesirable complication. As shown in the next section, the

analysis is concentrated on the region between this upper outflow and the main outflow below. The extent of mixing in region I roughly corresponds with the initial bulk Richardson number, Ri_0 , as would be expected. As shown in table 1(c), the value of Ri_0 decreases to values much less than unity as M_0 increases in these runs.

The $\hat{Q}(Z)$ curves for the 12° slope (figure 10c) show the same features as for 6° , but with greater magnitude. For most of these runs, $\hat{Q}(Z)$ increases further below $Z = 0$, reaching maxima in excess of 1.8 for some runs, near $Z = -0.2$. The $\hat{V}(Z)$ curves (figure 11c) show inflow near $Z = 0$ due to excess mixing in region I, and corresponding enhanced outflow above or near $Z = -0.4$. The oscillations in \hat{V} for small M_0 are again evident. The lower peak at $Z = Z_b$ (the main outflow) again decreases in amplitude and rises in elevation as M_0 increases, to the point ($M_0 > 0.08$) where it merges with the upper detrainment region and becomes indistinguishable from it. A small number of experiments were carried out with a slope of 20° . These showed \hat{V} profiles with a similar character to those at 12° .

The observations for 6° and 12° therefore show that the fluid mixed in region I is transported downslope to a level above or near $Z = -0.4$. From the observations it was not possible to determine which proportion of this transport was carried by the dense boundary current, and which was carried by the fluid external to it. The latter may well be significant. Fluid mixed at the upper boundary of these downflows mostly remains above the main current, and settles to its neutral density level. This implies downward motion and transport, to an extent that depends on the relative fractions of dense and ambient fluid in the mixture. Mixing in region I is mostly due to disturbances of Kelvin–Helmholtz type, where the fraction of dense fluid in the mixture is substantial. For instance, fluid that is mixed at $Z = 0$ and sinks to $Z = -0.3$ would contain 30% of dense fluid. In region II, however, the mixing processes are Holmboe-like. Here thin wisps of dense fluid penetrate the environment, and the fraction of dense fluid in the resulting mixture is small. This implies that the net external downslope motion and transport here is correspondingly small, and this is consistent with video observations of the flow in region II carried out for most runs. Downflow external to the main current is neglected in the next section, in which entrainment and detrainment are assumed to depend on properties of the downflow at the same level.

5. Entrainment and detrainment processes and coefficients

E_e , E_d and k are expected to be functions of the local values of M , Ri and θ , and in this section we use the results described in §4 to infer the forms of this functional dependence based on (3.24)–(3.26). We first need to be able to evaluate M and Ri as defined by (1.4), as functions of s or $Z (= -s \sin \theta / D)$. For this purpose, \bar{d} is readily measured for each run, $\hat{Q}(Z)$ is obtained as in §4, and $G(Z)$ is obtained as follows. If E_e is assumed to be a known function of s , the solution of (3.26) may be written

$$G(s) = G_0 h(s) - N^2 \sin \theta h(s) \int_0^s \frac{1}{h(s)} ds, \quad (5.1)$$

where

$$h(s) = \exp \left[- \int_0^s \frac{E_e(s')}{\bar{d}} ds' \right], \quad (5.2)$$

and $G = G_0 \equiv g'_0$ at $s = 0$ (in the experiments, $G(0)$ may differ slightly from g'_0 because of processes on the shelf etc., but we assume that this difference is not significant). We

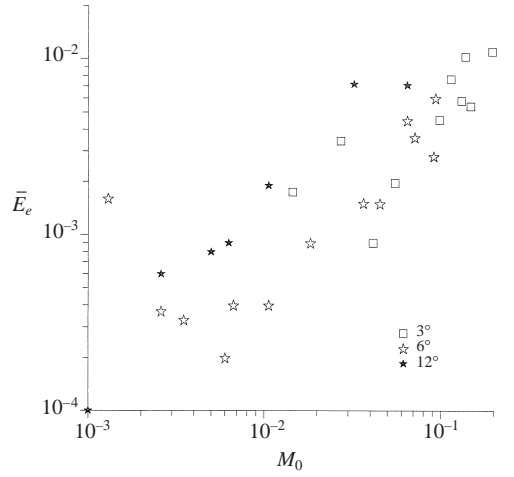


FIGURE 12. The mean entrainment coefficient \bar{E}_e as a function of M_0 .

may obtain successive approximations to $G(s)$ by using the fact that E_e is generally small. For the first of these, we assume that E_e is zero and obtain

$$G(s) = G_0 - N^2 \sin \theta s, \tag{5.3}$$

which vanishes where $s = G_0/(N^2 \sin \theta)$, or $z = -D$. An improvement on this may be obtained by assuming that E_e is constant with s , giving

$$G = G_0 \exp(-E_e s/\bar{d}) - \frac{N^2 \bar{d} \sin \theta}{E_e} (1 - \exp(-E_e s/\bar{d})). \tag{5.4}$$

We may determine a mean value of E_e by using the condition that $G = 0$ at the level where the fluid in the downflow becomes neutrally buoyant, at $Z = Z_b = -s_b \sin \theta/D$. We identify this depth with the level of the maximum in the main outflow, at the bottom of the downflow. We may then define this mean value \bar{E}_e for E_e by writing

$$h(s_b) = \exp \left[- \int_0^{s_b} \frac{E_e(s')}{\bar{d}} ds' \right] = \exp(-\bar{E}_e s_b/\bar{d}). \tag{5.5}$$

Using this form in (5.1) with $G(s_b) = 0$ gives a transcendental equation for \bar{E}_e in terms of Z_b and $\bar{d} \sin \theta/D$, namely

$$Z_b = -\ln(1 + \sigma)/\sigma, \quad \text{where } \sigma = \bar{E}_e/(\bar{d} \sin \theta/D). \tag{5.6}$$

Values of \bar{E}_e obtained by this procedure show a systematic increase with M_0 , as shown in figure 12.

These values of \bar{E}_e may then be used for E_e in (5.4) to give an approximation to $G(s)$ in the range $0 < s < s_b$, or $Z_b < Z < 0$, for each run. If E_e is quite small, as it is in most runs, (5.4) will capture most of the variation of $G(s)$ for the purpose of evaluating M and Ri to sufficient accuracy. These may be used to determine forms for E_e in terms of M and Ri that may then be used in (5.1) to obtain more accurate values of $G(s)$; in principle, this procedure may be continued iteratively, but this is not done here. Profiles of M and Ri using $G(s)$ from (5.4) with the values of \bar{E}_e for E_e , are shown in figure 13 for some representative runs for the slopes 3° , 6° and 12° .

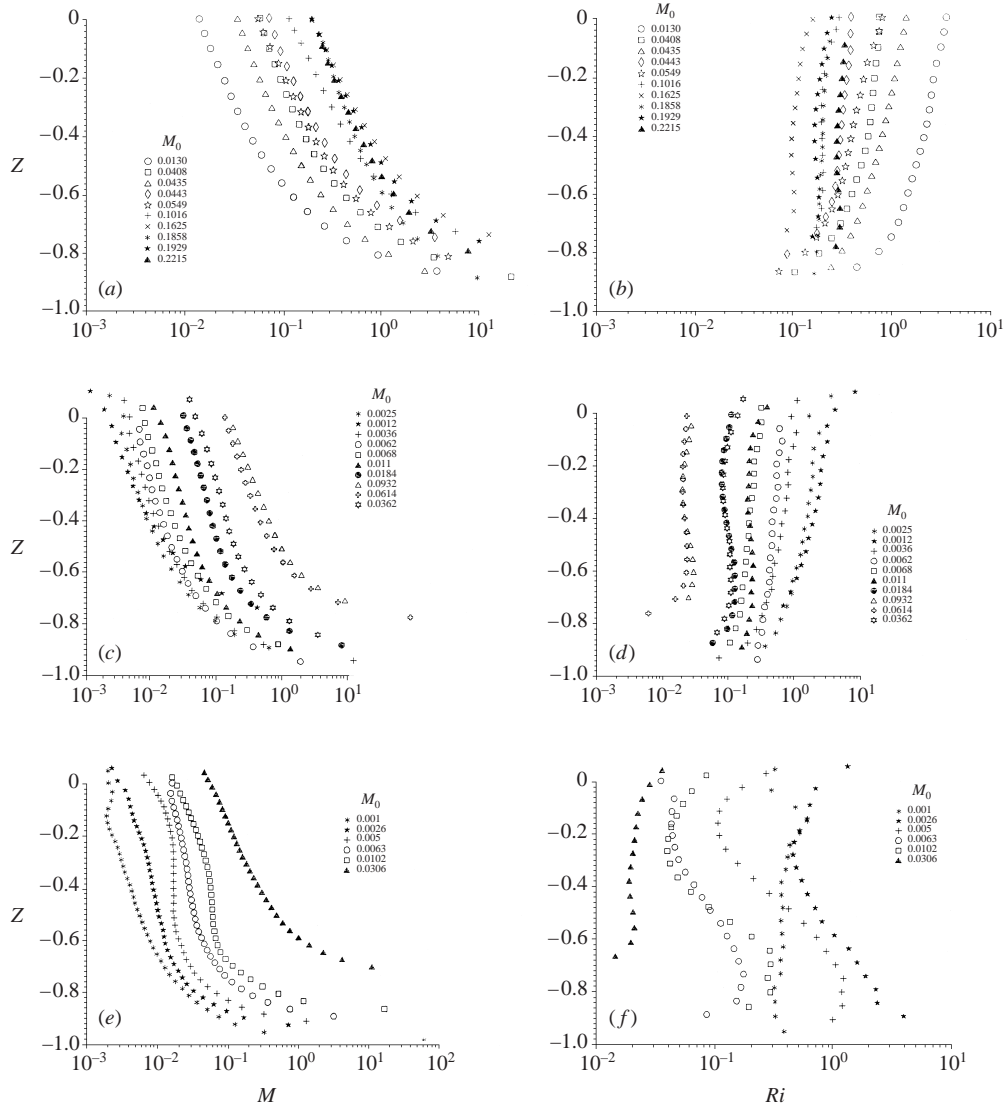


FIGURE 13. Profiles of Ri and M with depth Z for various slope angles. (a) M at 3° , (b) Ri at 3° , (c) M at 6° , (d) Ri at 6° , (e) M at 12° , (f) Ri at 12° . For each run, the data contain 200 points (approximately) covering the range $-1 < Z < 0$, and only every fifth point is plotted here. The values of Ri have been computed using the values of \bar{d} given in table 1(a, c, d).

These cover the range from $Z = 0$ down to the lowest minimum in \hat{V} before the final peak. In general, M increases monotonically with distance downward, but the behaviour of the Richardson number is more varied—for some runs at 3° and 6° it is approximately constant, for others it decreases monotonically, and for most 12° runs it oscillates with depth.

We now proceed to obtain expressions for E_d , E_e and k in terms of M , Ri and θ from the data, for region II below the influence of region I. In spite of these restrictions, this is a very extensive region covering at least half the downflow in most cases. We begin with $E_d - E_e$, which may be determined from (3.24) as a function of

Z or M in the form

$$E_d - E_e = -\frac{\bar{d}}{Q} \frac{\partial Q}{\partial s} = -\frac{\bar{d} \sin \theta}{D \hat{Q}} \frac{\partial \hat{Q}}{\partial Z} = -\frac{\bar{d} \sin \theta \hat{V}}{D \hat{Q}}, \quad (5.7)$$

since the quantities on the right-hand side have all been determined by observation. Profiles of $-(\hat{V}/\hat{Q})\bar{d}/D$ are shown plotted against M in figure 14 on a log-log scale for slope angles 3° , 6° and 12° . Only the ranges where \hat{V} is negative have been included here, down to the minimum in $|\hat{V}|$ just above the main outflow; this includes most of the downflow, as figure 11 shows. For each run, the ordinate $(E_d - E_e)/\sin \theta$ rises rapidly from a small value, and then appears to asymptote to a common power law relationship. Since M increases with distance downslope, the initial rise is interpreted as a rapid adjustment by the turbulence and mixing to an equilibrium state that depends on the local value of M , which is then maintained throughout the remainder of region II of the downflow. These curves appear to show that $(E_d - E_e)/\sin \theta$ is determined by the local value of M in each case, and increases monotonically with it. In contrast, as figure 13 shows, Ri does not vary monotonically with depth, and its behaviour may differ from run to run. Plots of $(E_d - E_e)/\sin \theta$ against Ri show considerable scatter between runs, with no systematic variation, and for some runs $E_d - E_e$ varies considerably while Ri varies hardly at all. This behaviour appears to exclude any explicit dependence of $E_d - E_e$ on Ri . For each slope angle, if the initial rapid rise region for each run is excluded, the data may be fitted with a power law relationship of the form

$$E_d - E_e = BM^\alpha \sin \theta. \quad (5.8)$$

The parameters α and B have been determined for each slope angle, including the observations at 4.5° . There is considerable scatter in the results, as seen in figure 14, and there is a suggestion that α decreases as θ increases, but this trend is not regarded as significant. Hence mean values of B and α have been chosen for all four slope angles, and overall the asymptotic line may be reasonably fitted by

$$B = 0.2 \pm 0.05, \quad \alpha = 0.4 \pm 0.1. \quad (5.9)$$

With these values for α and B , equation (5.8) is shown as the straight line fit to the asymptotic form of the data with increasing M , in figures 14(a), 14(b) and 14(c). Equations (5.8) and (5.9) then give a relationship for $E_d - E_e$ that is applicable to the main body of the downflow, namely region II.

We next determine the functional form of $E_e(M, Ri, \theta)$. This is not straightforward, because we do not have direct observations of E_e as a function of depth. For guidance we may look to the work of Ellison & Turner (1959), who established that the entrainment coefficient E_h for homogeneous flows is a decreasing function of the bulk Richardson number Ri . This is because the local value of the Richardson number controls the stability of the flow to infinitesimal disturbances, and the bulk Richardson number Ri controls the degree of turbulence and mixing resulting from growing disturbances in unstable flows. E_h is represented to good accuracy by (Turner 1986)

$$E_h = \frac{0.08 - 0.1Ri}{1 + 5Ri}, \quad (5.10)$$

but this implicitly assumes that entrainment for $Ri > 0.8$ is negligible, and this range is important in these experiments. An equivalent approximate expression that covers

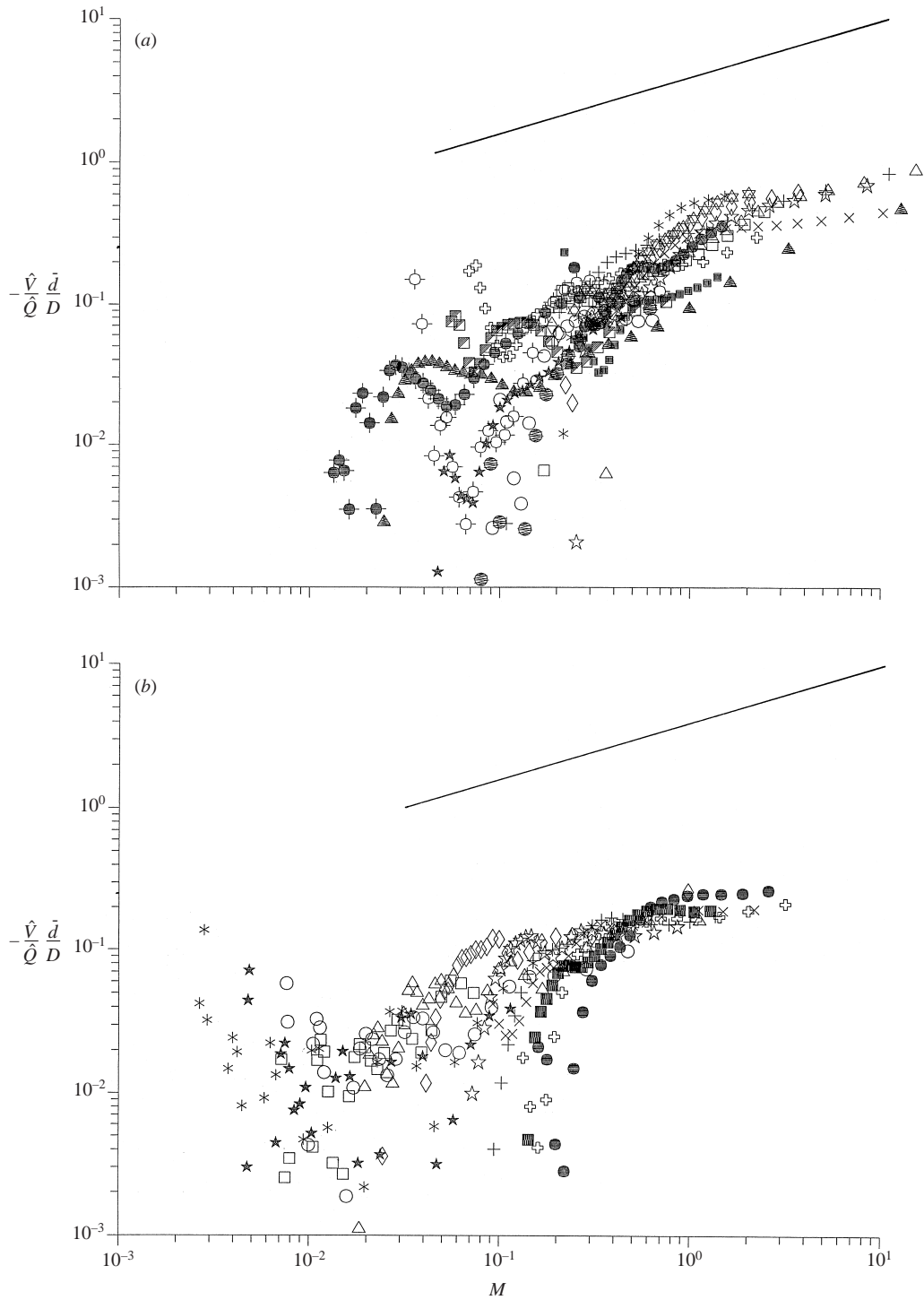


FIGURE 14 (a, b). For caption see facing page.

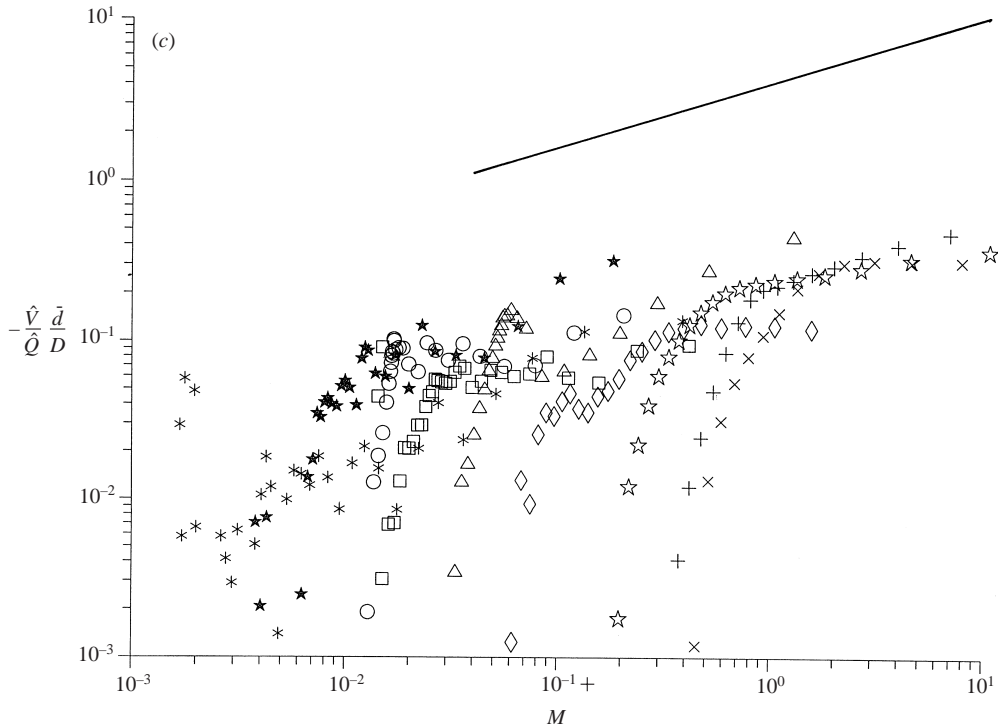


FIGURE 14. Plots of the function $-(\hat{V}/\hat{Q})\bar{d}/D = (E_d - E_e)/\sin\theta$ as a function of the local M value, for all runs for the slope angles (a) 3° , (b) 6° and (c) 12° . The plotted points denote every fifth datum point as in the previous figure. The straight lines denote the estimated asymptote for increasing M for all curves, corresponding to $\alpha = 0.4$ (see equation (5.9)). The asymptotes are displaced upwards for clarity—the actual asymptotes pass through the point (1, 0.2).

the range of $Ri > 0.1$ is (Lofquist 1960; Turner 1973; Fernando 1991)

$$E_h \approx \frac{0.001}{Ri}. \quad (5.11)$$

As discussed in § 3, E_h is defined differently from E_e , but its behaviour indicates that we may expect E_e also to be a decreasing function of Ri , and for the same physical reasons. The entrainment of fluid into the downflow depends on the local turbulent eddies, which are characterized by Ri , and are not sensitive to the environmental stratification. Hence the value N of the stratification should be of secondary importance, and so should M .

Figure 12 shows that \bar{E}_e may be roughly described by $\bar{E}_e \approx 0.1M_0^\gamma$, where $\gamma \leq 1$. However, M_0 and Ri_0 are not entirely independent, since

$$Ri_0 = \frac{G_0\bar{d}^3}{Q_0^2} = \frac{G_0D^3}{Q_0^2} \left(\frac{\bar{d}}{D}\right)^3 = \frac{1}{M_0^2} \left(\frac{\bar{d}}{D}\right)^3. \quad (5.12)$$

As shown in figure 9, \bar{d}/D shows an approximate power law relationship with M_0 , with a mean exponent of about 0.5. Hence the mean value of E_e , \bar{E}_e , is a decreasing function of Ri_0 , and for the 6° and 12° slopes in particular, may be approximately described by

$$\bar{E}_e \approx \frac{\text{const}}{Ri_0}. \quad (5.13)$$

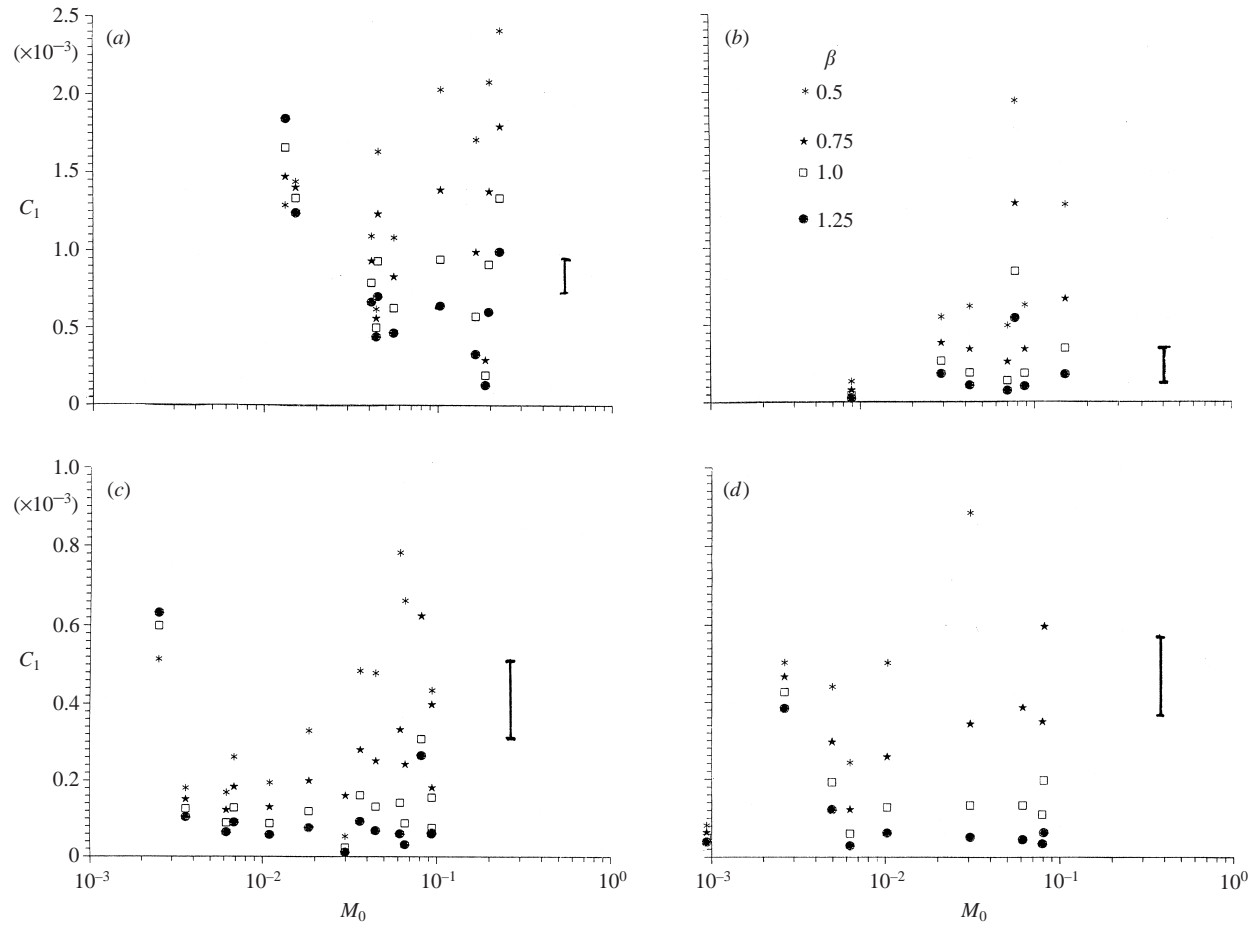


FIGURE 15. For caption see facing page.

For many of the 3°, 4.5° and 6° runs the variation in Ri with Z is small, and this suggests that an expression of this sort applies generally between E_e and Ri , with no explicit dependence on M . Accordingly we fit the expression

$$E_e = C_1 Ri^{-\beta}, \quad (5.14)$$

where C_1 is a constant, by integrating it over Z for each run for the slope angles of 3°, 4.5°, 6° and 12°, in the form

$$\bar{E}_e = \frac{1}{|Z_{min}|} \int_{Z_{min}}^0 E_e dZ = \frac{C_1}{|Z_{min}|} \int_{Z_{min}}^0 \frac{dZ}{Ri^\beta}, \quad (5.15)$$

for each of the values of $\beta = 0.5, 0.75, 1.0$ and 1.25 . Z_{min} is taken to be the level of the lowest minimum in $|\hat{V}|$, immediately above the main outflow, which assumes that negligible entrainment occurs below this level. The value of C_1 is then determined by equating the resulting value of \bar{E}_e with the observed value, and the objective is to find values of C_1 and β that apply to all runs for each slope angle. Note that this calculation includes both region I and region II. The results of these calculations are shown in figure 15. We consider first the runs with slope angles 3°, 6° and 12°. In general, the choice of $\beta = 1.0$ provides the best fit for all three slope angles. It could be argued that $\beta = 1.25$ is almost as good, but it is clear that $\beta = 0.5, 0.75$ give much greater scatter and are not satisfactory. With $\beta = 1.0$ the least-squares fit gives a mean value of $C_1 = 0.00012$ for both the 6° and 12° slopes (figures 15c and 15d). There are some large values of C_1 at the low Reynolds number end of the range, and these are disregarded as containing different physics and not relevant to the turbulent high Reynolds number regime. Excluding this range, the scatter of C_1 values about this mean is of order $\pm 20\%$, and is uniform with M_0 . The same is found for the 3° runs, excluding the runs with $Re \leq 350$, except that here there is more scatter and the mean value for $C_1 = 0.0008$. This value is close to the value 0.001 in equation (5.11), for horizontal flows ($\theta = 0^\circ$) in homogeneous environments. We may expect the same value to also apply here in this limit, since any effect of external stratification should be small for horizontal flows.

This difference in the magnitude of the entrainment coefficient for 3° and 6° by a factor of nearly seven for the same value of Ri is surprising, and has been investigated further by carrying out the series of runs at 4.5° slope. These are shown in figure 15(c), and mostly conform to a mean intermediate value of 0.00025, except for some large values at the high end of the range, of order 0.001. This is taken to imply that the value of C_1 is sensitive to the slope angle in this range of small values, with a rapid transition from values of order 0.001 near zero slope, to values of order 0.00012 for slopes greater than 5°. The data suggest, and it is reasonable to suppose, that C_1 is not sensitive to θ at the origin. This implies that horizontal flows are not sensitive to very small slope angles, and this is assumed here. It is noteworthy that the observations of \bar{d}/D for $\theta = 4.5^\circ$ shown in figure 9 indicate a different trend with M_0 from the others, with the values resembling those for 6° for small M_0 , and those for 3° at large M_0 . The data points for C_1 are shown in figure 16, together with a simple piecewise-smooth

FIGURE 15. The parameter C_1 in the inverse power law expression for E_e in terms of Ri , for various values of the exponent $\beta = 0.5, 0.75, 1.0, 1.25$ (equation (5.15)), for the bottom slopes (a) 3°, (b) 4.5°, (c) 6°, (d) 12°. Note that (a) and (b) have a common scale that differs from that for (c) and (d).

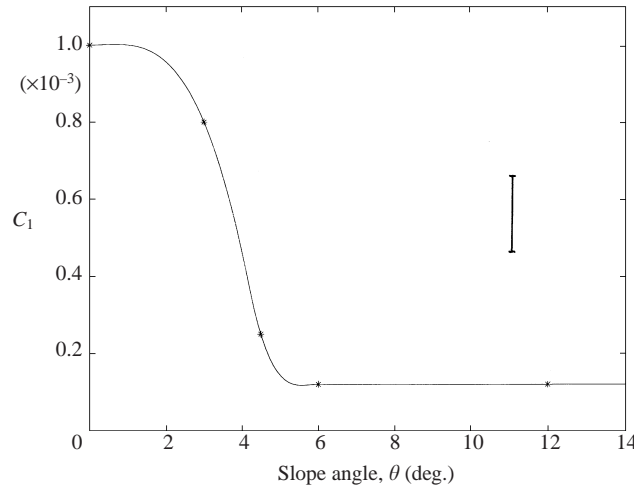


FIGURE 16. Observational points for the entrainment factors C_1 and the piecewise smooth fit for interpolation (equation (5.16)).

fit to these points, given by

$$\begin{aligned} C_1(\theta) &= 0.001 + 10^{-5}(1.3689\theta^2 - 1.1970\theta^3), & 0 < \theta < 4.1^\circ, \\ &= 0.00012 - 10^{-5}(2.1714(\theta - 6)^2 + 5.2995(\theta - 6)^3), & 4.1^\circ < \theta < 6^\circ, \\ &= 0.00012, & \theta > 6^\circ. \end{aligned} \quad (5.16)$$

This expression should be regarded as approximate, determined as it is by five mean values and assumed zero gradients at the origin and 6° . The upper limit of the range of θ for this expression is also uncertain, but these experiments indicate that it extends at least to 12° . Hence the expression for the entrainment coefficient is

$$E_e = \frac{C_1(\theta)}{Ri}. \quad (5.17)$$

From (5.8), the detrainment coefficient E_d is then given by

$$E_d = \frac{C_1(\theta)}{Ri} + 0.2M^{0.4} \sin \theta. \quad (5.18)$$

We next consider the drag term in the momentum equation (3.25), which may be estimated as follows. Detrainment of fluid from the downflow implies a loss of momentum, with a flux of magnitude $E_d U \rho U$, where $U = Q/\bar{d}$. On the other hand, entrainment incorporates fluid with no momentum into the current, and hence does not add a corresponding term. Hence we may write

$$k = E_d + C_{DU}, \quad C_D = C_{DL} + C_{DU}, \quad k + C_{DL} = E_d + C_D, \quad (5.19)$$

where C_{DU} represents drag on the upper surface that is not associated with an exchange of fluid. C_D represents the total drag apart from that due to fluid transfer. This is primarily associated with the drag of the rigid lower surface (and sidewalls), so that $C_{DU} \ll C_{DL}$, and is dependent on Re . Measurements by Lofquist (1960) of flow of a dense layer over a horizontal surface beneath a deep homogeneous upper layer indicate that a suitable approximate form for this in the present circumstances

is (fitted to data in figure 5 of Lofquist's paper)

$$\begin{aligned} C_D &= 7/Re_{ex}, & Re_{ex} &\leq 10^3, \\ &= 0.0556/Re_{ex}^{0.3}, & 10^3 &< Re_{ex} < 10^4, \end{aligned} \quad (5.20)$$

where Re_{ex} is an extended Reynolds number defined by

$$Re_{ex} = Re/(1 + 2\bar{d}/b), \quad (5.21)$$

where b is the breadth of the tank. Equation (5.20) is convenient but is probably an underestimate of the drag, partly because it takes no account of the stratification in the environment.

With these expressions for k and C_D , (3.25) may be expressed in the form

$$(Ri - 1) \frac{\partial \bar{d}}{\partial s} = E_d - 2E_e - C_D(Re_{ex}) + Ri \left(\tan \theta + \frac{E_e}{2} + \frac{\sin \theta}{2} \left(\frac{RiM^2}{\cos \theta} \right)^{1/3} \right). \quad (5.22)$$

From the steady-state experiments, where the variation of \bar{d} with s is observed to be very small, we may infer that the terms on the right-hand side collectively vanish, giving an expression for Ri in terms of M , θ and Re_{ex}

$$Ri = \frac{C_D(Re_{ex}) + C_1(\theta)(1/Ri - \frac{1}{2}) - 0.2M^{0.4} \sin \theta}{\tan \theta (1 + \frac{1}{2}(RiM^2 \cos^2 \theta)^{1/3})} \approx \frac{C_D(Re_{ex})}{\tan \theta} - 0.2M^{0.4} \cos \theta. \quad (5.23)$$

This expression may then be used to give a diagnostic relation for \bar{d} from

$$\bar{d} = \left(\frac{Q^2 Ri}{G \cos \theta} \right)^{1/3}. \quad (5.24)$$

The variations in Ri seen in figure 13(b,d,f) may now be understood as due to changes in Re_{ex} and M between runs, and with downslope position. Re_{ex} decreases and M increases with downslope distance, and the relative constancy of Ri at small slope angles is due to a balance between these two factors in (5.23).

6. Conclusions and discussion

Several novel features of flows down gentle slopes ($\leq 12^\circ$) into stratified environments have been described, as follows.

1. The downflow consists primarily of a boundary current with a sharp upper interface, maintained by the tendency of mixed fluid to find its own level in the stratified environment.

2. The flow contains three main regions, denoted I, II and III, ordered by distance downslope. Region I is an initial adjustment region, and region II comprises most of the current, in which the dense downflow has approximately constant mean thickness. It continuously loses fluid to the environment (detrainment) and gains it due to entrainment. In region III the fluid remaining at the end of the downflow finds its own neutral level.

3. Three distinct flow regions may also be identified with increasing distance normal to and above the slope. The first is the dense downflow itself, bounded by the interface; the second is the mixing region above the downflow; and the third is the external environment, which contains some motion due to the movement of partially mixed fluid finding its neutral level.

4. For small values of $M_0 (< 0.01)$, periodic small-scale variation with z in the net detrainment is observed. These variations are attributed to the effect of columnar disturbance modes on mixing, where these modes have been excited by the concentrated main outflow in region III.

5. Mixing in region I can be substantial, increasing \hat{Q} above unity and causing a broad upper level maximum in net outflow. This effect increases with slope angle, and is most noticeable at 12° in these experiments. These experiments have not been exhaustive, and some of these features deserve further study.

A model for turbulent downslope flows into stratified environments, based on observations of flow in region II, has been derived and is represented by equations (3.6), (3.16) and (3.21), which may be expressed as

$$\frac{\partial \bar{d}}{\partial t} + \frac{\partial Q}{\partial s} = (E_e - E_d) \frac{Q}{\bar{d}}, \quad (6.1)$$

$$\frac{\bar{d}}{Q} \frac{\partial G}{\partial t} + \frac{\partial G}{\partial s} = -N^2 \sin \theta - E_e G / \bar{d}, \quad (6.2)$$

$$\begin{aligned} \frac{\bar{d}^2}{Q^2} \frac{\partial Q}{\partial t} + (Ri - 1) \frac{\partial \bar{d}}{\partial s} = & E_d - 2E_e - C_D(Re_{ex}) \\ & + Ri \left(\tan \theta + \frac{E_e}{2} + \frac{\sin \theta}{2} \left(\frac{Ri M^2}{\cos \theta} \right)^{1/3} \right), \end{aligned} \quad (6.3)$$

with E_e and E_d given by (5.17) and (5.18). This model incorporates the effects of mixing, and constitutes an integrable system. For steady flow, \bar{d} has been observed to be constant, and by using this, (6.3) can be replaced by a diagnostic equation for \bar{d} from (5.23), (5.24). These functional relationships have been determined for a uniform slope, but the resulting expressions should also be applicable to non-planar slopes and regions of variable stratification, where θ and/or N vary with s , provided that this variation is sufficiently gradual for the turbulence to adjust in a quasi-static manner.

The forms of the variation of E_e , E_d and k with M , Ri and θ contain information about the nature of the turbulent eddies that accomplish the transfers. The dependence of $E_d - E_e$ on M and θ is not surprising: larger slope angles and stronger environmental stratification imply larger detrainment per unit length of slope. The fact that E_e decreases monotonically with increasing Ri is also consistent with previous models (Fernando 1991), and can be understood from the common expectation that Ri controls the rate of growth of unstable disturbances, and hence the consequent mixing events—smaller Ri implies greater instability. However, the reason why the parameter C_1 (and hence E_e for constant Ri) decreases with increasing slope angle requires some discussion. For horizontal flow ($\theta = 0^\circ$), such as in a conventional gravity current driven by an imperceptible pressure gradient, the maximum shear in the flow occurs at the density interface. The resulting disturbances have the form of Kelvin–Helmholtz instabilities and billows, and are generally symmetric about this interface. These properties are only slightly affected if the upper flow is stratified. However, for the case of flow down a slope of inclination 6° or greater, the mean velocity and density profiles are driven by buoyancy and have the form shown in figure 17. Here the maximum in the shear occurs above the interface. This profile is also subject to shear instability with the resulting eddies concentrated near the maximum mean shear gradient, above the interface (Baines & Mitsudera 1994; Baines 1995). These

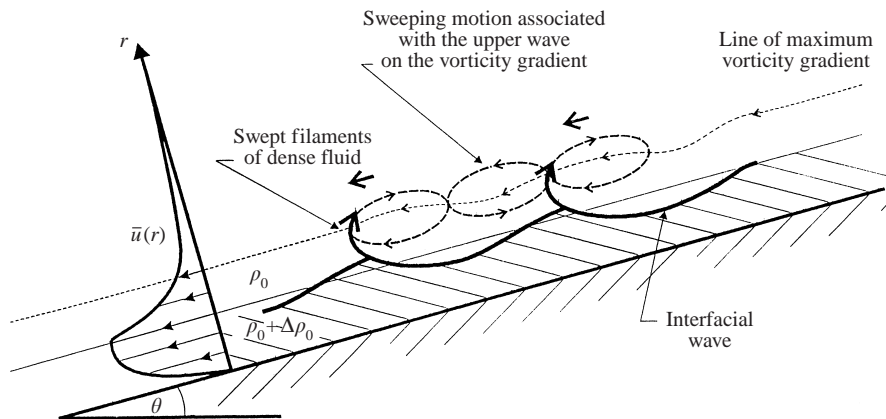


FIGURE 17. A schematic diagram showing the mean velocity profile in region II for 6° slope, and the process of Holmboe instability, which is due to the mutual interaction between a gravity wave on the interface and a vorticity wave on the vorticity gradient above it (see Baines & Mitsudera 1994; Baines 1995). The main dynamical forces maintain the mean velocity and density profiles, so that the instability process keeps recurring, and wisps of detained fluid result. r here denotes the coordinate normal to the slope.

eddies sweep the interface and detach wisps of fluid from it, as may be seen in figures 3(b) and 3(c). Accordingly, their capacity for mixing fluid within the downflow is considerably reduced when compared with that of eddies that coincide with the maximum in density gradient. This mixing is quantitatively represented by equation (5.17), and the difference is reflected in the value of the entrainment coefficient C_1 , which varies by an order of magnitude between 0° and 6° .

Other authors have noted sensitivity of the behaviour of dense fluid released on slopes to the slope angle, when the latter is small. Changes in the flow when the slope increases from zero to angles greater than about 5° have been described by Britter & Linden (1980) for gravity current heads, and by Beghin, Hopfinger & Britter (1981) for negatively buoyant clouds. These experiments were for homogeneous environments, and showed the change from a near-horizontal gravity current dominated by bottom friction, to near thermal-like behaviour, dominated by buoyancy and mixing with the environment.

The ranges of values M , Ri and θ covered in the present experiments are very large (see figure 13), and generally include those realized in larger-scale environmental flows. This suggests that the mixing parameterizations (5.17), (5.18) may be applicable to these situations. Specific examples are katabatic flows down hillsides (e.g. Manins & Sawford 1979) and over the Antarctic continent (Schwerdtfeger 1984; Pettré & André 1991), driven by radiative cooling in the atmosphere, and for deep flows in the ocean (e.g. Price & Baringer 1994; Baines & Condie 1998). One important parameter is the drag coefficient $C_D(Re)$, which decreases with increasing Re to a value of about 0.004 (Garratt 1992). For the flows described by the present model, (5.23) implies that Ri must also decrease with increasing Re , implying greater mixing. It also implies that the model should break down if C_D is sufficiently small, or the slope angle is sufficiently large, since Ri must be positive. In the present experiments, this angle was found to be between 12° and 30° , with the flows at steeper angles having more of the character of a turbulent plume than of the downslope gravity current described here. Experiments with this different regime have been carried out and will be reported elsewhere.

The author is most grateful for the efforts of David Murray, who has played a major role in the experiments and data analysis, to Mark Hibberd for a critical review, and to anonymous referees for constructive comments.

REFERENCES

- BAINES, P. G. 1995 *Topographic Effects in Stratified Flows*. Flows. Cambridge University Press.
- BAINES, P. G. 1999 Downslope flows into a stratified environment—structure and detrainment. In *Mixing and Dispersion in Stably Stratified Flows: Proc. 5th IMA Conf. on Stratified Flows, Dundee* (ed. P. A. Davies), pp. 1–21.
- BAINES, P. G. & CONDIE, S. 1998 Observations and modelling of Antarctic downslope flows: a review. In *Ocean, Ice and Atmosphere: Interactions at the Antarctic Continental Margin*, AGU Antarctic Research Series Vol. 75 (ed. S. S. Jacobs & R. Weiss), pp. 29–49.
- BAINES, P. G. & MITSUDERA, H. 1994 On the mechanism of shear flow instabilities. *J. Fluid Mech.* **276**, 327–342.
- BEGHIN, P., HOPFINGER, E. J. & BRITTER, R. E. 1981 Gravitational convection from instantaneous sources on inclined boundaries. *J. Fluid Mech.* **107**, 407–422.
- BRITTER, R. E. & LINDEN, P. F. 1980 The motion of the front of a gravity current travelling down an incline. *J. Fluid Mech.* **99**, 532–543.
- ELLISON, T. H. & TURNER, J. S. 1959 Turbulent entrainment in stratified flows. *J. Fluid Mech.* **6**, 423–448.
- FERNANDO, H. J. S. 1991 Turbulent mixing in stratified fluids. *Ann. Rev. Fluid Mech.* **23**, 455–493.
- GARRATT, J. R. 1992 *The Atmospheric Boundary Layer*. Cambridge University Press.
- IMBERGER, J., THOMPSON, R. O. R. Y. & FANDRY, C. B. 1976 Selective withdrawal from a finite rectangular tank. *J. Fluid Mech.* **78**, 489–512.
- LIST, E. J. & IMBERGER, J. 1973 Turbulent entrainment in buoyant jets and plumes. *Proc. ASCE, J. Hydraul. Div.* **99**, 1461–1474.
- LOFQUIST, K. 1960 Flow and stress near an interface between stratified liquids. *Phys. Fluids* **3**, 158–175.
- MANINS, P. C. & SAWFORD, B. L. 1979 Katabatic winds: a field case study. *Q. J. R. Met. Soc.* **105**, 1011–1025.
- MITSUDERA, H. & BAINES, P. G. 1992 Downslope gravity currents in a continuously stratified environment: a model of the Bass Strait outflow. *Proc. 11th Australasian Fluid Mechanics Conference, Hobart, Australia*, pp. 1017–1020.
- MONAGHAN, J. J., CAS, R. A. F., KOS, A. M. & HALLWORTH, M. 1999 Gravity currents descending a ramp in a stratified tank. *J. Fluid Mech.* **379**, 39–70.
- MORTON, B. R., TAYLOR, G. I. & TURNER, J. S. 1956 Turbulent gravitational convection from maintained and instantaneous sources. *Proc. R. Soc. Lond. A* **234**, 1–23.
- PETTRÉ, P. & ANDRÉ, J.-C. 1991 Surface-pressure change through Loewe's phenomena and katabatic flow jumps: study of two cases in Adélie Land, Antarctica. *J. Atmos. Sci.* **48**, 557–571.
- PRESS, W. H., FLANNERY, B. P., TEUKOLSKY, S. A. & VETTERLING, W. T. 1986 *Numerical Recipes*. Cambridge University Press.
- PRICE, J. F. & BARINGER, M. O. 1994 Outflows and deep water production by marginal seas. *Prog. Oceanogr.* **23**, 161–200.
- SCHWERTFEGER, W. 1984 *Weather and Climate of the Antarctic*. Elsevier.
- SIMPSON, J. E. 1997 *Gravity Currents: in the Environment and the Laboratory*, 2nd Edn. Cambridge University Press.
- SMITH, P. C. 1975 A streamtube model for bottom boundary currents in the ocean. *Deep-Sea Res.* **22**, 853–873.
- TURNER, J. S. 1973 *Buoyancy Effects in Fluids*. Cambridge University Press.
- TURNER, J. S. 1986 Turbulent entrainment: the development of the entrainment assumption, and its application to geophysical flows. *J. Fluid Mech.* **173**, 431–471.
- WONG, A. 1998 Stratification and circulation produced by turbulent plumes. PhD thesis, Australian National University.